Stem Cell Reports
Article
ISSCR
OPEN ACCESS

MSX1^{+}PDGFRA^{low} limb mesenchyme-like cells as an efficient stem cell source for human cartilage regeneration

Yuansong Liao,[1,2] Fanchen Kang,[1,2] Jingfei Xiong,[1,2] Kun Xie,[1,2] Mingxu Li,[1,2] Ling Yu,[1,2] Yuqing Wang,[1,2] Hanyi Chen,[1,2] Guogen Ye,[1,2] Yike Yin,[1,2] Weihua Guo,[3,4] Haoyang Cai,[1,2] Qing Zhu,[1,2,*] and Zhonghan Li[1,2,3,4,5,*]

[1]Center of Growth Metabolism and Aging, Laboratory of Bio-Resource and Eco-Environment of Ministry of Education, Animal Disease Prevention and Food Safety Key Laboratory of Sichuan Province, College of Life Sciences, Chengdu, China
[2]Department of Anesthesiology, West China Second University Hospital, Key Laboratory of Birth Defects and Related Diseases of Women and Children of Ministry of Education, Sichuan University, Chengdu, China
[3]State Key Laboratory of Oral Disease, West China Hospital of Stomatology, Sichuan University, Chengdu, China
[4]National Engineering Laboratory for Oral Regenerative Medicine, West China Hospital of Stomatology, Sichuan University, Chengdu, China
[5]Lead contact
*Correspondence: zhuqing@scu.edu.cn (Q.Z.), zhonghan.li@scu.edu.cn (Z.L.)
https://doi.org/10.1016/j.stemcr.2024.02.001

SUMMARY

Degenerative bone disorders have a significant impact on global health, and regeneration of articular cartilage remains a challenge. Existing cell therapies using mesenchymal stromal cells (MSCs) have shown limited efficacy, highlighting the necessity for alternative stem cell sources. Here, we have identified and characterized MSX1^{+} mesenchymal progenitor cells in the developing limb bud with remarkable osteochondral-regenerative and microenvironment-adaptive capabilities. Single-cell sequencing further revealed the presence of two major cell compositions within the MSX1^{+} cells, where a distinct PDGFRA^{low} subset retained the strongest osteochondral competency and could efficiently regenerate articular cartilage *in vivo*. Furthermore, a strategy was developed to generate MSX1^{+}PDGFRA^{low} limb mesenchyme-like (LML) cells from human pluripotent stem cells that closely resembled their mouse counterparts, which were bipotential *in vitro* and could directly regenerate damaged cartilage in a mouse injury model. Together, our results indicated that MSX1^{+}PDGFRA^{low} LML cells might be a prominent stem cell source for human cartilage regeneration.

INTRODUCTION

Musculoskeletal conditions affect approximately 1.71 billion individuals and are the leading contributor to pain and disability worldwide (Cieza et al., 2021). With the aging population, the incidence of musculoskeletal conditions has continued to rise, and joint disorders such as osteoarthritis are most prevalent in people aged 65 years and older (Hunter et al., 2020; Long et al., 2020). Articular cartilage in the joint has severely limited capability to self-repair because of its distinct anatomy, with chondrocytes encased in an extracellular matrix composed of their secretions, such as collagens, proteoglycans, and other non-collagenous proteins, as well as the absence of a regional blood supply or neural innervations (Kwon et al., 2019). Thus, the majority of current clinical interventions focus on symptom relief and disease management (Arden et al., 2021; Katz et al., 2021) and progression, and patients are often left with no alternative options except surgery.

Cell-based therapies have been recognized as a prominent approach to restoring damaged articular cartilage. Currently, autologous chondrocyte implantation (ACI) is the only US Food and Drug Administration (FDA)-approved cellular treatment (Makris et al., 2015). However, its practicality is limited by several risk factors, such as donor site morbidity due to chondrocyte harvesting, periosteal hypertrophy, surgery-related complications, and age-related concerns (Harris et al., 2010; Madeira et al., 2015). Meanwhile, other stem cells, including mesenchymal stromal cells (MSCs) from multiple sources (Le et al., 2020; Liu et al., 2022; Madeira et al., 2015; McGonagle et al., 2017), skeletal stem cells (SSCs) (Murphy et al., 2020; Ono et al., 2019; Serowoky et al., 2020), and neural crest stem cells (NCSCs) (Achilleos and Trainor, 2012; Dash and Trainor, 2020; Liu and Cheung, 2016), were also being explored pre-clinically and clinically to examine their potential use in cartilage regeneration. Among these cells, MSCs were one of the most intensively studied stem cells in cartilage regeneration, but the results were often less encouraging, with a high incidence of fibrosis tissue formation reported in a clinical trial using endogenous bone marrow-derived MSCs (BM-MSCs) (Steadman et al., 2003) and abnormal cartilage repair observed in 76% patients when using exogenous ones (Koh et al., 2014). One of the key issues for the use of MSCs for cartilage regeneration is its lack of developmental relevance to the joint chondrocytes. Even for BM-MSCs, joint cartilage was already formed when MSCs were harvested, indicating that MSCs and cartilage chondrocytes were at distinct developmental stages, despite MSCs' capability to differentiate into

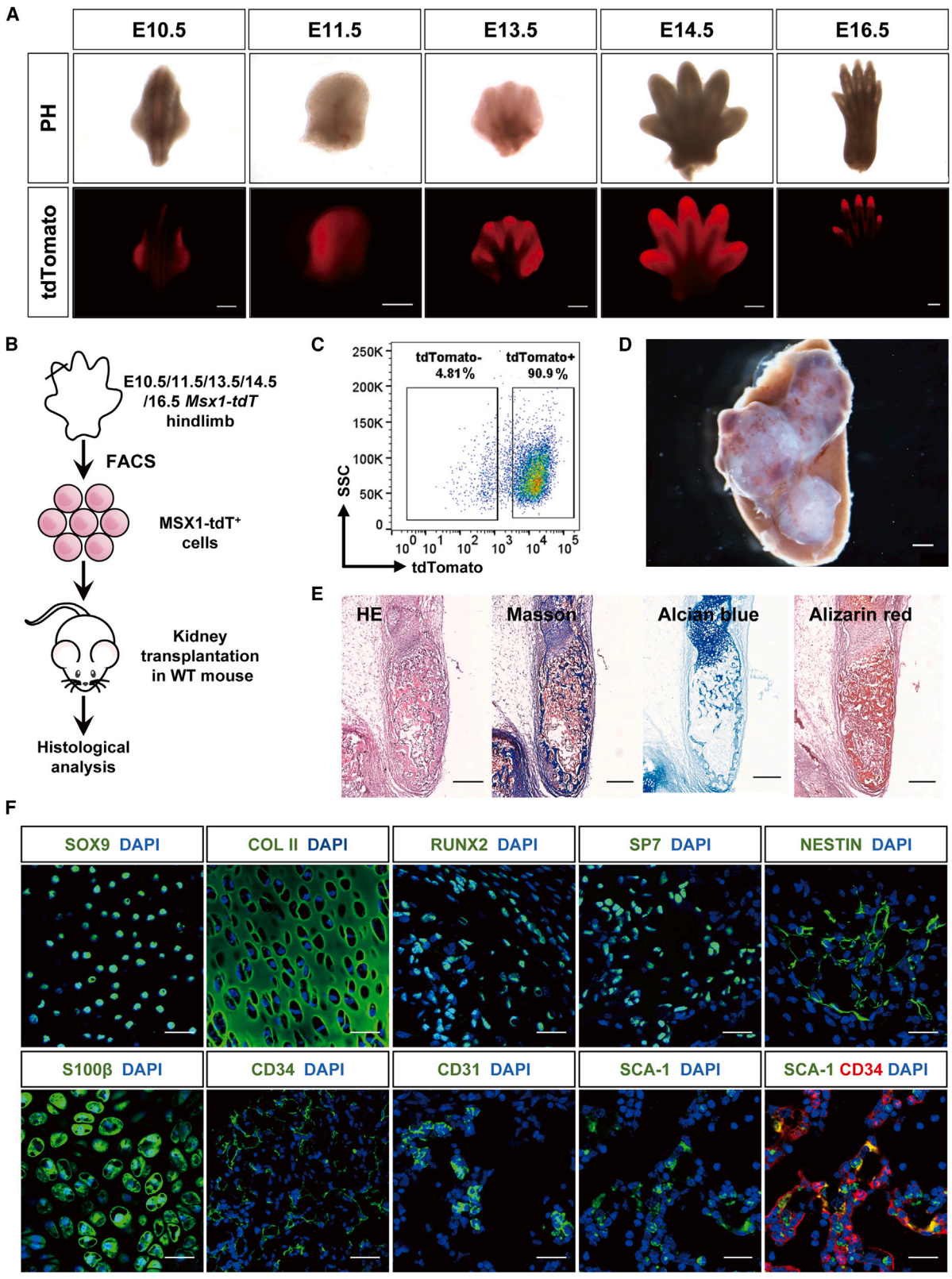

(legend on next page)

chondrocytes *in vitro*. Thus, there is growing enthusiasm to explore and test other more developmentally relevant stem cell sources for cartilage regeneration.

During development, mammalian synovial joint cartilages were formed during the endochondral ossification process of condensed mesenchymal cells in the osteochondral primordium through interzone formation and joint cavitation (Chijimatsu and Saito, 2019). The cell origin of joint cartilage was typically derived from three lineages: neural crest, sclerotome, and lateral plate mesoderm (LPM) (Humphreys et al., 2022). Among them, mesenchymal progenitor cells from LPM give rise to all the appendicular skeleton, such as the radius, humerus, femur, and tibia (Prummel et al., 2020). In mice, the formation of limb buds marks the initial development of the appendicular skeleton, where an interplay of Wnt, Sonic hedgehog (SHH), FGF, and retinoic acid (RA) signaling pathways determines the further patterning and formation of limb bones and cartilage (McQueen and Towers, 2020; Royle et al., 2021). Interestingly, it was found that the transcription factors Msx1 and Msx2 played critical roles in early limb bud development (Bensoussan-Trigano et al., 2011; Lallemand et al., 2005), and Msx1$^+$ mesenchymal progenitors were the key mediator for digit tip regeneration (Lehoczky et al., 2011). Recent publication of single-cell analysis on developing limb bud also indicated *Msx1*, as well as *Lhx2* and *Lhx9*, marked the naive progenitor population (Markman et al., 2023), suggesting that MSX1$^+$ cells might be a potential cell source for osteochondral regeneration. However, the regenerative capabilities of these cells were not systematically investigated yet and neither was the strategy to derive them from human pluripotent stem cells (hPSCs) established.

In this study, we used a *Msx1*$^{P2A\text{-}tdTomato}$ knock-in reporter mouse model established previously (Hu et al., 2022) to investigate the regenerative potential of limb-bud-derived MSX1$^+$ mesenchymal cells across multiple developmental stages and discovered that MSX1$^+$ progenitors from E10.5 possessed remarkable osteochondral-regenerative and microenvironment-adaptive capabilities. Single-cell RNA sequencing (scRNA-seq) with fate mapping further revealed that two major cell compositions were present in these cells, where a distinct PDGFRA^{low} subset retained the strongest osteochondral competency and could efficiently regenerate articular cartilage *in vivo*. Furthermore, we developed a strategy to generate MSX1$^+$PDGFRA^{low} limb mesenchyme-like (LML) cells from hPSCs that closely resemble their mouse counterparts. These cells were bipotential *in vitro* and able to directly regenerate damaged cartilage in a mouse injury model. Together, our findings indicated that MSX1$^+$PDGFRA^{low} LML cells might be a prominent stem cell source for human cartilage regeneration.

RESULTS

Primary MSX1$^+$ mesenchymal progenitors from limb buds exhibited strong osteochondral-regenerative capabilities

Previously, we constructed a *Msx1*$^{P2A\text{-}tdTomato}$ knockin mouse in which Msx1 expression was tracked through P2A-mediated tdTomato expression (Hu et al., 2022). The tdTomato expression was observed throughout early limb development from embryonic day 10.5 (E10.5) to E16.5 (hindlimb), where it was initially expressed broadly across the limb bud primordium and gradually concentrated on interdigital and distal digit tip regions (Figures 1A and S1A). To evaluate the developmental potential of these cells, MSX1$^+$ cells were sorted by flow cytometry from mouse hindlimb at various stages (E10.5, E11.5, E13.5, E14.5, and E16.5) and transplanted into renal capsules of the recipient mice (Figures 1B, 1C, and S1B). Three weeks post-transplantation, large areas with bone-like structures were formed in the transplanted regions (Figures 1D, S1B, and S1C), especially for E10.5 MSX1$^+$ cells, which yielded the largest grafts and positive

Figure 1. Limb bud MSX1$^+$ mesenchymal progenitors exhibited strong bone regeneration capability

(A) Expression pattern of MSX1 (tdTomato) in primary hindlimbs of different developmental stages. Scale bars: 500 μm.

(B) Schematic illustration of limb bud MSX1$^+$ (tdTomato$^+$) mesenchymal progenitor cells transplantation *in vivo*. MSX1$^+$ cells isolated from the mouse primary hindlimbs (E10.5, E11.5, E13.5, E14.5, and E16.5 hindlimbs) were first dissociated into single cells and embedded in collagen I for incubation overnight at 37°C. These cells were then transplanted into the kidney capsule of recipient C57BL6 WT mice. Samples were harvested for analysis at three weeks post-transplantation.

(C) Isolation of E10.5 MSX1$^+$ limb bud mesenchymal progenitors by flow cytometry.

(D) Representative image of bone-like tissues formed by transplanted MSX1$^+$ cells under the kidney capsule. Samples were harvested at three weeks post-transplantation. Scale bar: 1 mm.

(E) H&E, Masson, Alcian blue, and alizarin red staining confirmed the presence of collagen, proteoglycan, and calcium salts in the bone-like tissues in MSX1$^+$ cell transplants. Scale bars: 250 μm.

(F) Immunostaining of osteochondral markers in the regenerated bone-like tissues. Chondrocytes: SOX9 and COL II; osteoblasts: RUNX2 and SP7; neural lineage: NESTIN and S100β; vascular endothelial cells (VECs): CD31 and CD34; hematopoietic and stromal cells: SCA-1. Scale bars: 25 μm (SOX9, COL II, RUNX2, and SP7) and 30 μm (NESTIN, S100β, CD31, CD34, and SCA-1).

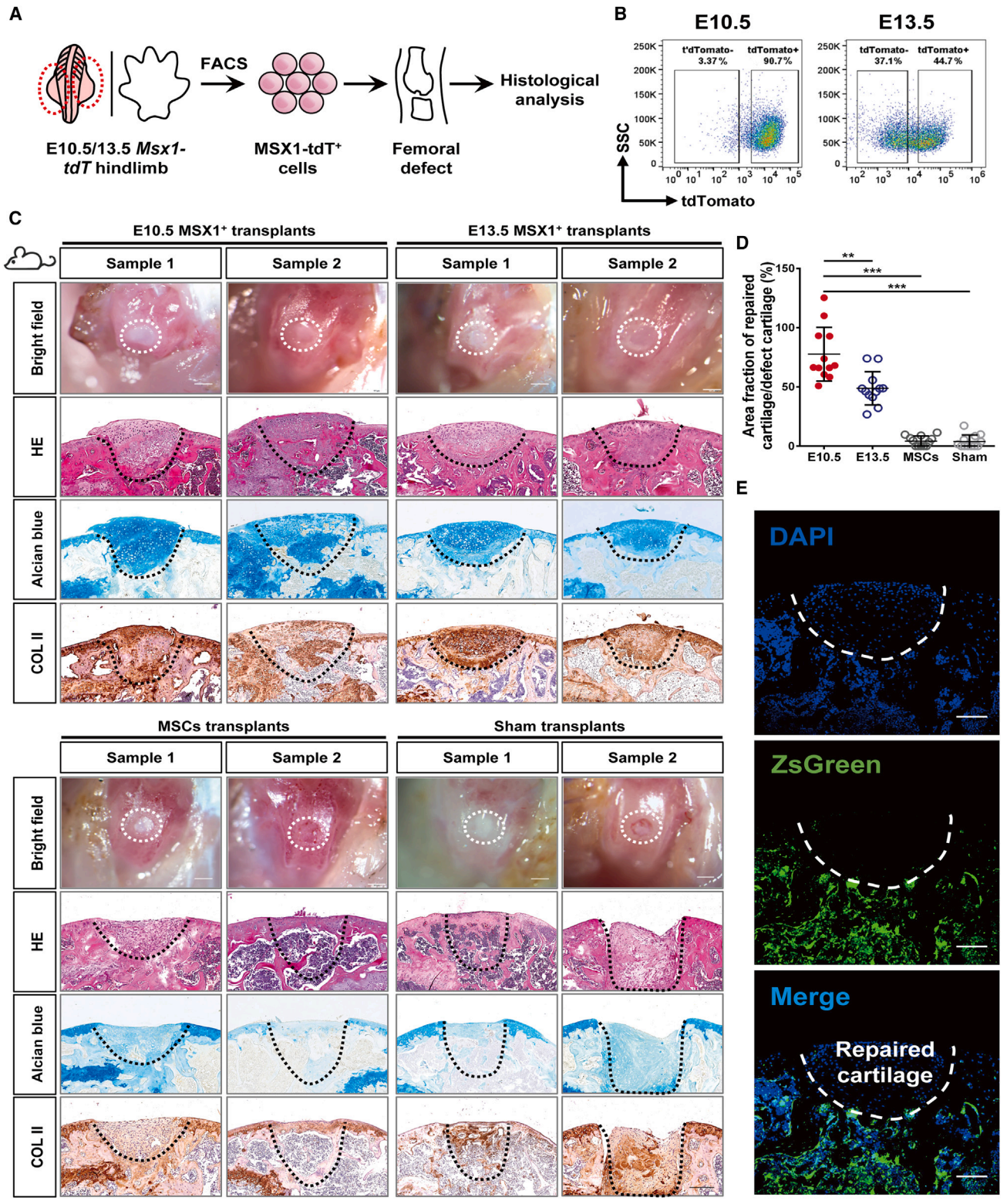

Figure 2. Microenvironmental adaption of MSX1+ mesenchymal progenitors enabled efficient articular cartilage regeneration

(A) Schematic illustration of limb-bud-derived MSX1+ (tdTomato+) mesenchymal progenitor cells transplantation in the articular cartilage injury model. MSX1+ cells isolated from E10.5 and E13.5 hindlimbs were embedded in collagen I for incubation overnight before being

(legend continued on next page)

staining for Masson, Alcian blue, and Alizarin red (Figure 1E), suggesting them at a more progenitor state. Immunostaining in the graft sections further revealed the expression of various markers, including SOX9 and collagen II (COL II) for chondrocyte and cartilage (Bi et al., 1999; Lefebvre et al., 1997), RUNX2 and SP7 for osteoblasts (Franceschi and Xiao, 2003; Hojo et al., 2016), NESTIN and S100β for stromal (Bernal and Arranz, 2018) and neural cells (Carr and Johnston, 2017), and vascular endothelial cell makers CD31 and CD34, as well as hematopoietic stem cell (HSC) and stromal marker SCA-1 (Tokoyoda et al., 2010; Wilson and Trumpp, 2006) (Figure 1F). Co-localization of SCA-1 and CD34 indicated the association between potential HSCs and endothelial cells (Figure 1F).

To investigate whether the cells in the grafts were derived from the transplanted ones, sorted MSX1$^+$ cells were transplanted in a ZsGreen reporter mouse, in which all the host cells were labeled as ZsGreen$^+$ (Figure S1D). Indeed, most regions of the MSX1$^+$ graft were ZsGreen$^-$ (Figure S1E). Immunostaining of bone, cartilage, neural, and vascular markers further confirmed that most bone and cartilage signals were from MSX1$^+$ cells, while ~25%–35% of neural and vascular ones were from the host (Figures S1F and S1G). Moreover, quantitative analysis of the grafts from different MSX1$^+$ cell transplants revealed that MSX1$^+$ cells from E10.5 limb buds had the highest regenerative capabilities (Figure S2). Together, these data indicated that MSX1$^+$ mesenchymal progenitor cells from the developing limb bud possessed strong osteochondral induction potential and could regenerate bone/cartilage-like tissues efficiently upon transplantation.

Limb-bud-derived MSX1$^+$ mesenchymal progenitors could directly repair defects in the joint cartilage

To investigate if the limb-bud-derived mesenchymal progenitors were able to respond to microenvironmental cues and directly regenerate cartilage without prior induction for chondrocyte lineage commitment, MSX1$^+$ cells from E10.5 and 13.5 limb buds were sorted using fluorescence-activated cell sorting (FACS) and transplanted in a joint injury mouse model with 0.8 mm diameter critical sized articular cartilage damage (Figures 2A and 2B) (Fitzgerald et al., 2008). In comparison, besides sham control, MSCs isolated from compact bones were also included (Zhu et al., 2010). The expression of MSC markers as well as their osteochondral differentiation capacities were confirmed before use (Figure S3). Interestingly, three weeks post-transplantation, both E10.5 and E13.5 cells showed remarkable regenerative capabilities to repair the defect sites and form hyaline cartilage. However, the thickness of the cartilage layer was greater in the E10.5 group (Figures 2C and 2D). Histological analysis with Alcian blue staining and COL II immunostaining further confirmed the cartilage formation (Figure 2C). In contrast, the MSC and sham groups exhibited incomplete repair and formed fibrotic tissues but no cartilage (Figure 2C). To verify that the regenerated cartilage was derived directly from the transplanted MSX1$^+$ cells but not any host cells recruited to the damaged site, the experiments were repeated in the *H11-ZsGreen* transgenic mice, in which host cells would be visualized as ZsGreen$^+$. Indeed, the regenerated hyaline cartilages were completely derived from the transplanted MSX1$^+$ cells but not the host (Figure 2E).

Together, these data suggested that the primary limb-bud-derived MSX1$^+$ mesenchymal progenitors were highly adaptive to the local microenvironment, and upon transplantation in the joint region, could directly regenerate hyaline cartilage without recruitment of host cells.

scRNA-seq analysis revealed the osteochondral potential of limb-bud-derived MSX1$^+$PDGFRA^{low} progenitors

To investigate what cell populations within the developing limb buds might retain the osteochondral differentiation capabilities, single-cell transcriptome analysis was performed using E10.5 mouse limb buds (Figure 3A). Cluster analysis with UMAP (uniform manifold approximation and projection) identified seven cell subgroups, each with unique gene expression features (Figures 3B and 3C).

transplanted into the femoral defect sites of recipient mice. Samples were harvested for analysis at three weeks post-transplantation. Transplantation of MSCs was used for comparison. Animals transplanted with collagen matrix only were used as the sham control.

(B) Isolation of MSX1$^+$ mesenchymal progenitors by flow cytometry.

(C) MSX1$^+$ mesenchymal progenitors could efficiently regenerate articular cartilage at the injury site. Representative pictures of two samples with bright-field (BF; white dashed line) and H&E (black dashed line) tissue morphology are shown. Alcian blue and COL II staining were used to detect cartilage formation. Scale bars: 1 mm (BF) and 200 μm (H&E, Alcian blue, and COL II).

(D) Quantitative analysis of cartilage repair efficiency in defect sites. The results confirmed that E10.5 MSX1$^+$ cells had the most efficient regenerative potential. Error bars represent data from twelve sections of six mice from three independent experiments (mean ± SD). Statistics: one-way ANOVA followed by Tamhane's T2 post hoc multiple comparisons using SPSS version 22.0. **$p < 0.01$ and ***$p<0.001$.

(E) Regenerated articular cartilage was derived from transplanted MSX1$^+$ cells. Cells were transplanted in ZsGreen-expressing hosts to verify the cell origin of regenerated cartilage tissues. Immunofluorescence images showing repaired cartilage tissues were ZsGreen negative. Scale bars: 100 μm.

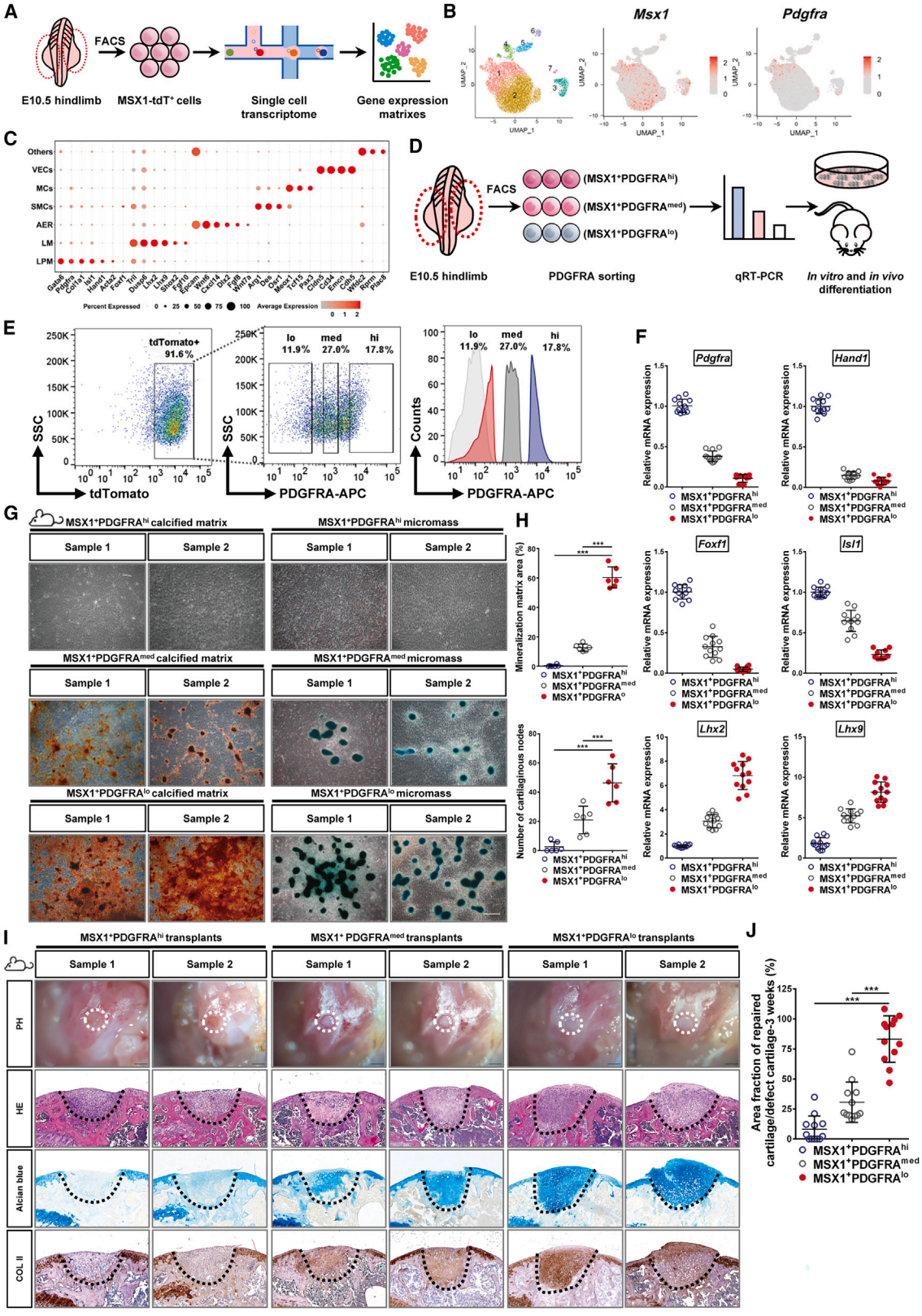

(legend on next page)

Among them, *Msx1* expression was detected in clusters 1, 2, and 3 (Figure 3B). Clusters 1 and 2 were further defined as LPM and limb mesenchyme (LM), respectively, on the basis of their marker expression (*Gata6*, *Pdgfra*, and *Hand1* in cluster 1; *Lhx2*, *Lhx9*, and *Dusp6* in cluster 2) (Figure 3C). Cluster 3 was defined as the apical ectodermal ridge (AER), as it expressed *Epcam*, *Wnt6*, and *Fgf8* (Figure 3C). Pseudotime analysis of mesenchymal cells, identified through *Prrx2* and *Twist-1* expression (Figure S4A), revealed a differentiation path from LPM to LM (Figures S4B–D), suggesting that LPM cells were at a more progenitor state in development. As LPM was positive for *Pdgfra* expression, which was also a surface marker (Figure 3C), we separated the limb-bud-derived MSX1$^+$ cells into three groups, PDGFRA^{high}, PDGFRA^{medium}, and PDGFRA^{low} (Figure 3D) and using FACS to enrich each cell population (Figure 3E). qRT-PCR analysis further confirmed correct cell sorting and demonstrated that MSX1$^+$PDGFRA^{high} cells were highly enriched with LPM markers such as *Foxf1*, *Hand1*, and *Isl1*, while MSX1$^+$PDGFRA^{low} cells were enriched with LM ones such as *Lhx2* and *Lhx9* (Figure 3F).

To evaluate the osteochondral competence of the sorted cells, *in vitro* differentiation assays for osteogenesis and chondrogenesis were carried out using sorted PDGFRA^{high}, PDGFRA^{medium}, and PDGFRA^{low} MSX1$^+$ cells. The results demonstrated that the MSX1$^+$PDGFRA^{low} cells retained the highest potential for both types of differentiation, as evidenced by the formation of more osteoblastic and cartilaginous nodules compared with the other two cells (Figures 3G and 3H). Renal capsule transplantation experiments further confirmed these findings, where MSX1$^+$PDGFRA^{low} cells gave rise to the largest bone-like tissues, while tissues formed by MSX1$^+$PDGFRA^{high} cells were the smallest (Figure S4E). It was further supported by quantitative measurement of the regenerated bone-like tissues (Figure S4F). To evaluate if the MSX1$^+$PDGFRA^{low} cells were also microenvironment adaptive, sorted cells were transplanted directly in the joint detect sites in the injury mouse model. Indeed, the cells exhibited remarkable cartilage regenerative potential, even without prior induction of chondrocyte lineage commitment (Figures 3I and 3J), and the regenerated cartilage was still maintained after 8 weeks (Figures S4G and S4H). Thus, these results indicated that among the primary cells derived from the developing limb buds, MSX1$^+$PDGFRA^{low} cells were the key progenitors that retained high osteochondral potential and could adapt to the local microenvironment and regenerate hyaline cartilage efficiently.

Stepwise induction of MSX1$^+$PDGFRA^{low} LML cells from hPSCs

To test if the developmental trajectory and cell compositions were conserved between human and mouse limb buds, we reanalyzed scRNA-seq data from human embryos at 5 weeks post-conception (WPC) (He et al., 2021). Hindlimb cells were identified through specific markers expressed at this stage, including *Pdgfra* and *Sox9* (Xi et al., 2020), as well as *Tbx4* (Ranganath et al., 2020) (Figure S5A). LPM and LM cells within the hindlimb populations and AER cells were further identified through their marker expression (LPM: *PDGFRA*$^{+-}$ *COL1A2*$^+$*COL3A1*$^+$*TSHZ2*$^+$; LM: *LHX2*$^+$*HOXC10*$^+$*HMMR*$^+$ *MKI67*$^+$; AER: *EPCAM*$^+$*FGF8*$^+$*DLX5*$^+$*KRT8*$^+$) (Figure S5B).

Figure 3. A distinct PDGFRA^{low} subset retained the osteochondral competency of MSX1$^+$ mesenchymal progenitors

(A) Schematic diagram showing scRNA-seq analysis of E10.5 limb bud MSX1$^+$ (tdTomato$^+$) mesenchymal progenitor cells.

(B) Seven cell clusters were identified from scRNA-seq analysis (UMAP plots). Expression of Msx1 and Pdgfra are shown.

(C) Specific marker expression of different cell clusters. Cluster 1: lateral plate mesoderm (LPM); cluster 2: limb mesenchyme (LM); cluster 3: apical ectodermal ridge (AER).

(D) Schematic diagram of MSX1$^+$ cell sorting and characterization strategy.

(E) Isolation of MSX1$^+$ subpopulations by cell sorting. Left: flow cytometry analysis of MSX1$^+$ cells from E10.5 embryos. Middle and right: gating strategy to isolate PDGFRA-expressing cells.

(F) qRT-PCR analysis of marker gene expressions for LPM (*Foxf1*, *Hand1*, *Pdgfra*, and *Isl1*) and LM (*Lhx2* and *Lhx9*) in sorted cells. Error bars represent data from four independent experiments with triplicates.

(G) Confirmation of the osteochondral competency of MSX1$^+$PDGFRA^{low} subpopulation *in vitro*. Differentiated cells from the sorted subsets were stained with alizarin red for osteogenic (left) and Alcian blue for chondrogenic lineages (right). Scale bars: 100 μm.

(H) Quantitative analysis of the differentiated mineralized matrix and cartilaginous nodes by sorted cells. MSX1$^+$PDGFRA^{low} cells formed the largest area of the mineralized matrix and the highest number of cartilage nodes. Error bars represent data from six samples of three independent experiments (mean ± SD). Statistics: one-way ANOVA followed by Tamhane's T2 (mineralized matrix) and Tukey (cartilaginous nodes) post hoc multiple comparisons using SPSS version 22.0. ***$p < 0.001$.

(I) MSX1$^+$PDGFRA^{low} cells could efficiently regenerate articular cartilage *in vivo*. Representative images of 3 week samples are shown. Alcian blue and COL II staining (black dashed line) were used to detect cartilage formation. Scale bars: 1 mm (BF) and 200 μm (H&E, Alcian blue, and COL II).

(J) Quantitative analysis of cartilage repair in the defect sites at 3 weeks. Error bars represent data from twelve sections of six mice in three independent experiments (mean ± SD). Statistics: one-way ANOVA followed by Tukey post hoc multiple comparisons using SPSS version 22.0. ***$p < 0.001$.

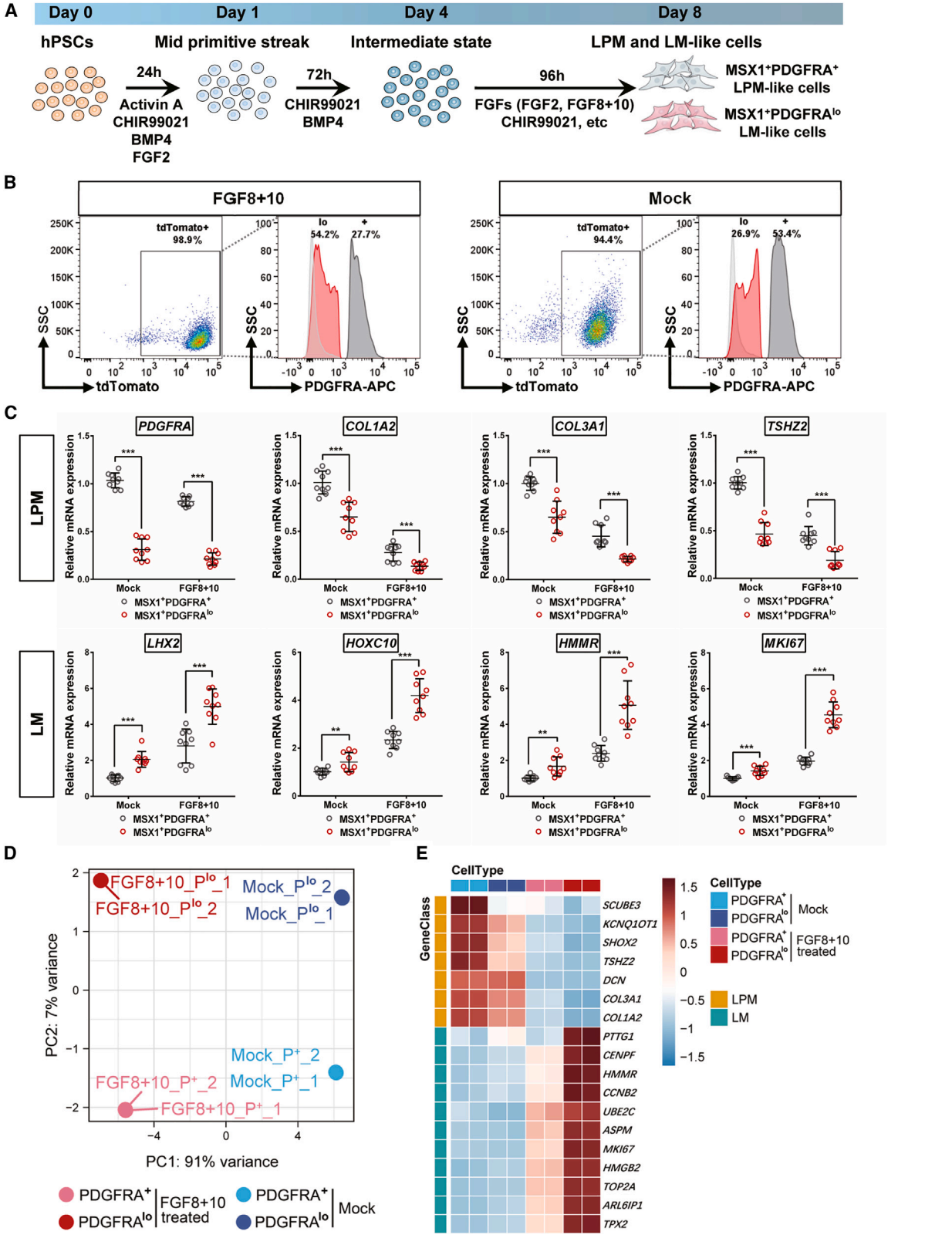

(legend on next page)

Pseudotime trajectory analysis indeed confirmed that similar developmental paths from LPM to LM were conserved in human cells as well (Figures S5C and S5D). Previously, it was reported that AER played a crucial role in the induction of LM in mouse limbs (Street et al., 2018). Therefore, we analyzed the ligand-receptor signals between the LM and AER cells. CellChat analysis (Jin et al., 2021) revealed that Wnts and FGFs were the main stimulating signals from AER to LM cells (Figure S5E), suggesting that the derivation of human LML cells from hPSCs might also require such signals.

To mimic human limb bud development *in vitro* and derive LML cells, a *MSX1:P2A-tdTomato* knockin hPSC cell line was first established by using CRISPR-Cas9 (Figure S6A) and confirmed by Sanger sequencing (Figure S6B). Immunostaining of OCT4 and SOX2 further confirmed the self-renewal state of the knock-in cell line (Figure S6C). To induce LML cells, hPSCs were first differentiated toward mid-primitive streak (MPS) by a cocktail of activin A, CHIR99021 (CHIR), FGF2, and BMP4 and then further induced to an intermediated state by CHIR and BMP4 only for three days before final differentiation using either CHIR99021 to activate Wnt signaling or FGFs (FGF2 or FGF8+10) to stimulate FGF signaling (Figure 4A). As limb bud development is a three-dimensional (3D) process characterized by distinct patterning along the proximal-distal (P-D), anterior-posterior (A-P), and dorsal-ventral (D-V) axes (Huangfu et al., 2008), we compared the effects of both traditional 2D culture and 3D culture using spheroid formation. After 8 days of differentiation, cells in all the treatment groups displayed various degrees of MSX1/tdTomato expression (Figure S6D). qRT-PCR analysis of marker genes for LPM (, PDGFRA, *COL1A2*, and *TSHZ2*), LM (*LHX2* and *HOXC9*), and general mesenchymal makers such as *HAND2* and *PRRX1*, as well as the hindlimb-specific marker *TBX4*, all confirmed that 3D spheroid culture exhibited stronger gene expression induction and the FGF8+10 group was the highest (Figure S6E). The presence of MSX1^{+}PDGFRA^{+} and MSX1^{+}PDGFRA^{low} cells was also evaluated by flow cytometry, where 3D-cultured FGF8+10 treated cells, together with mock control, were chosen for further characterization because of robust differentiation of both MSX1^{+}PDGFRA^{+} and MSX1^{+}PDGFRA^{low} cells (Figures 4B and S6F).

MSX1^{+}PDGFRA^{+} and MSX1^{+} PDGFRA ^{low} cells were separated by FACS and the expression of LPM and LM markers were analyzed using qRT-PCR (Figure 4C). For all the LM markers (*LHX2*, *HOXC10*, *HMMR,* and *MKI67*), MSX1^{+}PDGFRA^{low} cells from the FGF8+10 treated group exhibited stronger induction during differentiation than mock control (Figure 4C). Transcriptome analysis by RNA-seq comparing FGF8+10 and mock-derived cells further indicated that the cells were at distinct states and FGF8+10 treatment promoted the cells to differentiate toward a LML profile (Figures 4D and 4E). Together, our results indicated that by using 3D spheroid culture with FGF8+10 cytokine stimulation, hPSCs could be induced step by step to acquire LML state, and MSX1^{+}PDGFRA^{low} LML cells could be readily derived from such differentiation strategy.

Direct regeneration of joint hyaline cartilage by hPSC-derived MSX1^{+}PDGFRA^{low} LML cells

To evaluate the developmental potential and cartilage repair abilities of differentiated LPM-like and LML cells, we conducted both *in vitro* and *in vivo* differentiation assays using hPSC-derived MSX1^{+}PDGFRA^{+} and MSX1^{+}PDGFRA^{low} cells from the 3D-FGF8+10 group (Figure 5A). Indeed, compared with MSX1^{+}PDGFRA^{+} cells, MSX1^{+}PDGFRA^{low} LML cells exhibited stronger differentiation capabilities in both osteogenic and chondrogenic differentiation *in vitro* (Figure 5B), which were also supported by the quantitative measurement of the regenerated calcified matrix and chondrospheres (Figure 5C). We then transplanted both cells into a joint cartilage defect model and found that MSX1^{+}PDGFRA^{low} cells were also highly microenvironment adaptive, similar to their mouse counterparts, and could directly regenerate articular hyaline cartilage *in vivo* (Figure 5D). Quantification of the cartilage also confirmed the enhanced regeneration competency of MSX1^{+}PDGFRA^{low} cells

Figure 4. Induction of MSX1^{+}PDGFRA^{low} limb mesenchyme-like cells from human pluripotent stem cells

(A) Schematic illustration of the strategy for stepwise induction of MSX1^{+} cells from human pluripotent stem cells (hPSCs).

(B) FACS analysis confirmed the induction of MSX1^{+}PDGFRA^{+} LPM-like and MSX1^{+}PDGFRA^{low} LM-like cells from 3D-cultured *MSX1*$^{P2A\text{-}tdTomato}$ hPSCs with FGF8+10 and mock treatments.

(C) qRT-PCR analysis confirmed the stronger induction of LM markers in the FGF8+10 treated cells. LPM makers: *PDGFRA*, *COL1A2*, *COL3A1*, and *TSHZ2*. LM markers: *LHX2*, *HOXC10*, *HMMR*, and *MKI67*. Error bars represent data from three independent experiments with triplicates. Statistics: independent-sample t test using SPSS version 22.0. **p < 0.01 and ***p < 0.001.

(D) Principal component (PC) analysis of bulk RNA-seq data from hPSC-derived MSX1^{+}PDGFRA^{low} and MSX1^{+}PDGFRA^{+} cells. FGF8+10-treated cells were compared with mock control.

(E) Heatmaps of marker gene expression in FGF8+10 treated cells compared with mock control. The range of transcriptional expression is illustrated by a color change as depicted on the extreme right of the figure (dark red correlates to high expression, whereas light blue correlates to low expression).

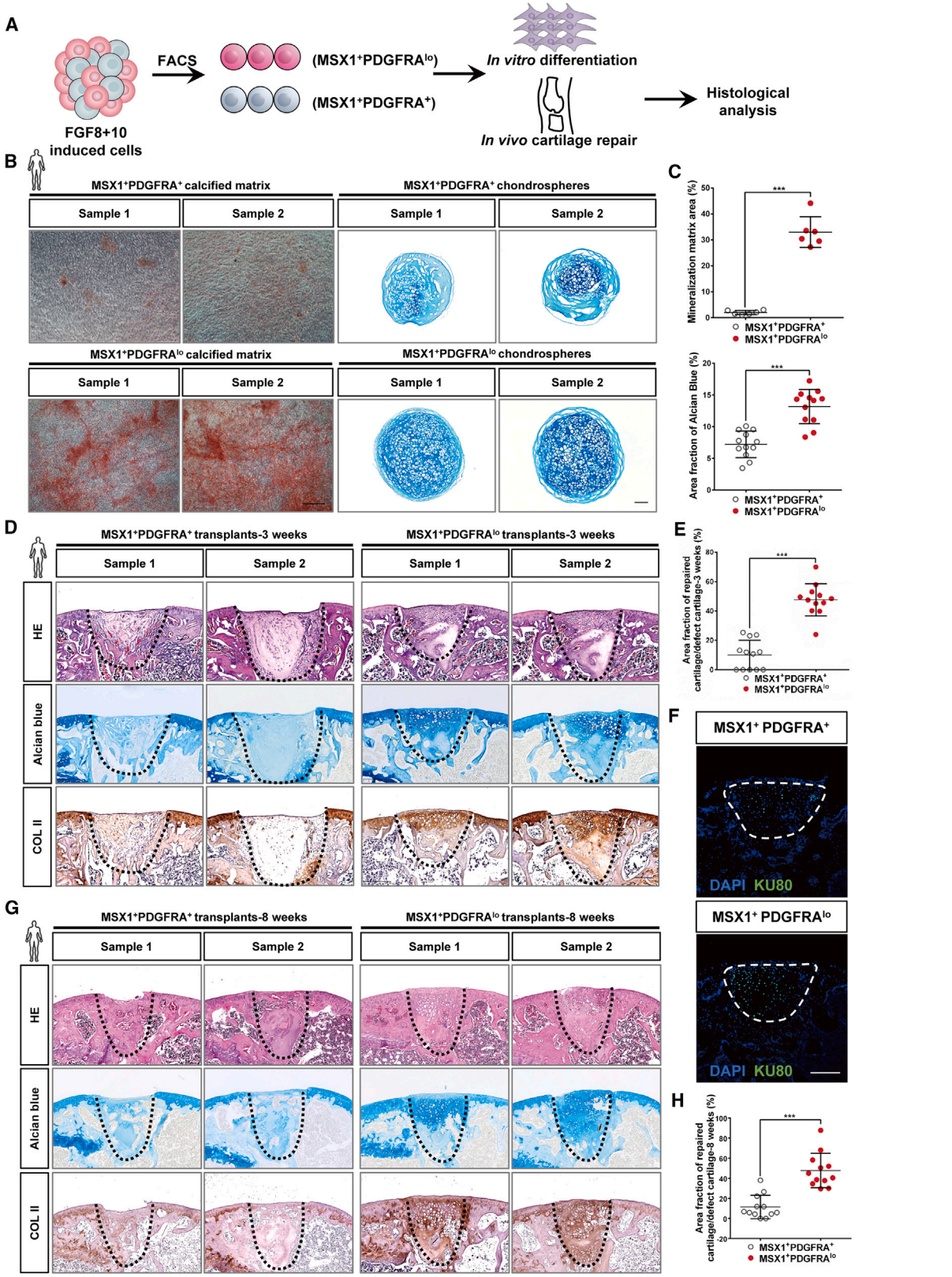

(legend on next page)

(Figure 5E). Immunostaining of human nuclear protein KU80 indicated that the repairment was not due to the recruitment of the host cells but by the transplanted cells themselves (Figure 5F). In addition, the regenerated cartilage was still maintained after 8 weeks post-transplantation (Figures 5G and 5H).

Thus, these results indicated that the hPSC-derived MSX1^{+}PDGFRA^{low} LML cells retained osteochondral biopotency and were highly microenvironment adaptive that could regenerate joint articular cartilage without prior induction of chondrocyte fate commitment.

DISCUSSION

Stem cell-based therapy holds great promise for cartilage regeneration, but identifying suitable seed cells remains a challenge. In the present study, we investigated the osteochondral potential of MSX1^{+} mesenchymal progenitors isolated from the developing mouse limb buds. Kidney capsule transplantation and animal injury model repairment assays confirmed that these cells retained remarkable osteochondral differentiation capabilities and could adapt to the joint microenvironment and regenerate hyaline cartilage without prior lineage induction. scRNA-seq and pseudotime analysis revealed the developmental trajectory of LPM to LM, where *Pdgfra* expression was a marker to separate the two populations. Subsequent characterization of LPM (MSX1^{+}PDGFRA^{high}) and LM (MSX1^{+}PDGFRA^{low}) cells further discovered that LM cells retained the strongest osteochondral potential, suggesting them as a promising cell source for cartilage repair. To derive LML cells from hPSCs, we developed a protocol with 3D culture and a combination of FGF8 and FGF10 to promote lineage commitment toward LM. Indeed, hPSC-derived MSX1^{+}PDGFRA^{low} LML cells exhibited robust osteochondral competency *in vitro* and could also adapt to the joint microenvironment and directly regenerate damaged cartilage *in vivo*. Therefore, our work highlighted the potential of MSX1^{+}PDGFRA^{low} LML cells as a promising cell source for hyaline cartilage regeneration (Figure 6).

Although MSCs have been widely studied for cartilage repair, their heterogeneity and limited expansion pose challenges to clinical translation. In contrast, hPSCs offer a potentially unlimited source of cells with the ability to differentiate into various lineages. Recent studies have shown that allogeneic primate iPSC-derived organoids elicited a minimal immune reaction in repairing articular cartilage defects (Abe et al., 2023), suggesting that hPSC-derived cells might be a viable option for cartilage repair. To identify the proper cell source, our initial research focused on early limb buds, which possessed the potential to develop into a complete limb and could regenerate osteoblasts, chondroblasts, and neural and endothelial cells. In addition, mouse limb bud cells demonstrated superior cartilage repair effects compared with compact bone-derived MSCs. More importantly, we were able to establish a differentiation strategy to derive MSX1^{+}PDGFRA^{low} LML cells from hPSCs and provide evidence that these cells were like their mouse counterparts in retaining the osteochondral potential.

Finally, it is worth noting that our differentiation strategy would also need further improvement, as the differentiation efficiency is limited currently. In addition to that, although hPSC-derived MSX1^{+}PDGFRA^{low} cells exhibited

Figure 5. MSX1^{+}PDGFRA^{low} LM-like cells exhibited strong osteochondral competence

(A) Schematic illustration for the strategy to characterize the osteochondral competence of hPSC-derived LM-like cells.

(B) Confirmation of osteogenic and chondrogenic capability of LPM- and LM-like cells *in vitro*. Stronger staining of alizarin red and Alcian blue was seen in LM-like cells (MSX1^{+}PDGFRA^{low}) in comparison with LPM-like ones (MSX1^{+}PDGFRA^{+}), suggesting the enhanced osteochondral potential of the LM-like cells. Scale bars: 100 μm.

(C) Quantitative analysis of the alizarin red (top) and Alcian blue (bottom) staining. Msx1^{+}PDGFRA^{low} cells had better potential to form more mineralized matrix and larger chondrospheres. Top: error bars represent data from six samples in three independent experiments (mean ± SD). Bottom: error bars represent data from twelve chondrospheres from three independent experiments (mean ± SD). Statistics: independent-sample t test using SPSS version 22.0. ***p < 0.001.

(D) Efficient regeneration of articular cartilage by LM-like cells *in vivo*. Representative images are shown. Alcian blue and COL II staining (black dashed line) were used to detect cartilage formation. Scale bars: 250 μm.

(E) Quantitative analysis of the regenerated cartilage. Alcian blue staining was performed in 3 week samples. Error bars represent data from twelve samples of three independent experiments (mean ± SD). Statistics: independent-sample t test using SPSS version 22.0. ***p < 0.001.

(F) Confirmation of human origin in the transplanted cells. Representative images of KU80 immunostaining (white dashed line) in the articular cartilage defect sites are shown. Scale bars: 250 μm.

(G) Repaired articular cartilages were maintained after 8 weeks. Alcian blue and COL II staining (black dashed line) were used to detect cartilage formation. Scale bars: 250 μm.

(H) Quantitative analysis of the regenerated cartilage. Error bars represent data from twelve samples of three independent experiments (mean ± SD). Statistics: independent-sample t test using SPSS version 22.0. ***p < 0.001.

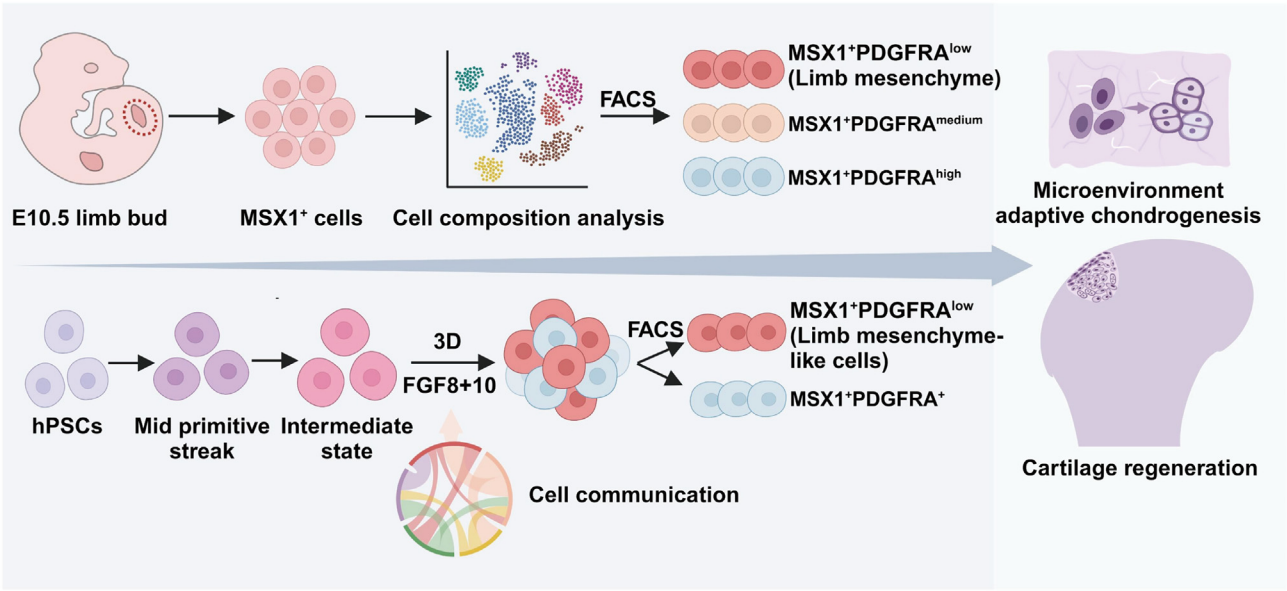

Figure 6. Illustrative model for limb mesenchyme-like cells as a promising stem cell source for cartilage regeneration

An important MSX1^{+}PDGFRA^{low} cell subpopulation was identified from mouse E10.5 hindlimb; these cells were remarkably osteochondral competent, were microenvironment adaptive, and could directly regenerate articular cartilage. A stepwise protocol was then developed to derive such cells from hPSCs, which is a promising approach for human cartilage regeneration.

upregulated expression of LM enriched signature genes when compared with MSX1^{+}PDGFRA^{+} counterparts, they did have differences from mouse primary limb mesenchymal cells. One such difference was that for mouse primary MSX1^{+}PDGFRA^{low} cells, their signature gene expressions were much stronger (usually 30- to 60-fold higher than MSX1^{+}PDGRFRA^{high} cells) and thus generally exhibited stronger osteochondral potential. This suggested that the differentiation protocol of hPSC to LM required further optimization. For example, AER cells are known to play critical roles in LM development by providing many inductive signals. Other signals secreted by AER besides FGF8+10 might have synergistic effects on LM derivation from hPSCs. Therefore, further investigations were warranted by combining those signals to derive more matured LML cells. Although our work was ongoing, it was reported that Prrx1^{+} limb bud-like mesenchymal cells were derived from hPSCs as well (Yamada et al., 2021), which exhibited the potential to form hyaline cartilaginous-like tissues *in vitro* and *in vivo*. However, these cells were induced by activating WNT but inhibiting BMP, TGF-β, and HH signaling, while in our case the cells were responsive to FGF8+10 induction, suggesting that the MSX1^{+}PDFGRA^{low} cells reported here might be more physiologically relevant. Meanwhile, both studies did support that LML cells derived from hPSCs could serve as a promising stem cell source for cartilage regeneration in humans.

EXPERIMENTAL PROCEDURES

Resource availability

Lead contact

Zhonghan Li (Zhonghan.Li@scu.edu.cn).

Materials availability

The materials included in this study are available upon reasonable request to the lead contact.

DATA AND CODE AVAILABILITY

The datasets generated in the present study are available from the lead contact upon reasonable request. The accession number for the scRNA-seq data reported in this paper is GEO: GSE232586.

Mouse strains and animal care

All animal experiments were approved by the Institutional Animal Care and Use Committee at the College of Life Sciences, Sichuan University. All animals were maintained under standardized conditions with the temperature and light controlled (25°C, 12 h light/dark cycle), in individually ventilated cages, and had free access to food and water. Knockin C57BL6-*Msx1*$^{P2A\text{-}tdTomato}$ mice and *H11-ZsGreen* mice were custom generated by Biocytogen, Inc. (Beijing, China). Mouse offspring from these strains were routinely genotyped using standard PCR protocols.

C57BL6 wild-type (WT) mice and NOD-SCID mice were purchased from GemPharmatech Co., Ltd. (Chengdu, China). C57BL6 WT mice were used as recipients for renal subcapsular and articular cartilage transplantation of mouse MSX1$^+$ cells, while NOD-SCID mice were used as recipients for articular cartilage transplantation of differentiated human LPM- and LML cells.

Single-cell preparation and scRNA sequencing of E10.5 MSX1$^+$ cells

About 20 hindlimb buds were dissected from E10.5 Msx1$^{P2A\text{-}tdTomato}$ mice. These limb buds were dissociated into single cells first and resuspended in PBS with 1% BSA. The sorted MSX1$^+$ cells were both counted and adjusted to the concentration of about 1 × 10^6/mL. Then the suspension was centrifuged at 550 × *g* for 5 min at 4°C and repeated twice. Cells were counted and cell viability was confirmed by Countess II Automated Cell Counter (catalog #AMQAX1000; Thermo Fisher Scientific). Samples were then used for scRNA-seq with the 10X Genomics system (library preparation and sequencing were performed by Berry Genomics Inc., Beijing, China).

Other experimental procedures can be found in supplemental information.

SUPPLEMENTAL INFORMATION

Supplemental information can be found online at https://doi.org/10.1016/j.stemcr.2024.02.001.

ACKNOWLEDGMENTS

We would like to thank the Core Facilities in the College of Life Sciences and College of Polymer Sciences & Engineering for their technical assistance. This work was supported by the National Key Research and Development Program of China (grants 2022YFA1104401 and 2021YFA1100601), the National Natural Science Foundation of China (grants 32071455 and 32271295), SCU grant 020SCUNL109, the Research and Development Program of West China Hospital of Stomatology Sichuan University (grant RD-03-202106), and the Fundamental Research Funds for the Central Universities (grant SCU2019D013).

AUTHOR CONTRIBUTIONS

Z.L., Q.Z., and Y.L. conceived the study. Y.L., J.X. K.X., and L.Y. performed most of the wet experiments. F.K., H.C., and H.C. performed the bioinformatic analysis. Y.W. and G.Y. provided experimental assistance. Z.L., Q.Z., H.C., W.G., and Y.Y. oversaw the collection of results and data interpretation. Z.L., Q.Z., and Y.L. wrote the manuscript. All authors have seen and approved the final version of the paper.

DECLARATION OF INTERESTS

The authors declare no competing interests.

Received: May 17, 2023
Revised: February 1, 2024
Accepted: February 1, 2024
Published: February 29, 2024

REFERENCES

Abe, K., Yamashita, A., Morioka, M., Horike, N., Takei, Y., Koyamatsu, S., Okita, K., Matsuda, S., and Tsumaki, N. (2023). Engraftment of allogeneic iPS cell-derived cartilage organoid in a primate model of articular cartilage defect. Nat. Commun. *14*, 804. https://doi.org/10.1038/s41467-023-36408-0.

Achilleos, A., and Trainor, P.A. (2012). Neural crest stem cells: discovery, properties, and potential for therapy. Cell Res. *22*, 288–304. https://doi.org/10.1038/cr.2012.11.

Arden, N.K., Perry, T.A., Bannuru, R.R., Bruyère, O., Cooper, C., Haugen, I.K., Hochberg, M.C., McAlindon, T.E., Mobasheri, A., and Reginster, J.-Y. (2021). Non-surgical management of knee osteoarthritis: comparison of ESCEO and OARSI 2019 guidelines. Nat. Rev. Rheumatol. *17*, 59–66. https://doi.org/10.1038/s41584-020-00523-9.

Bensoussan-Trigano, V., Lallemand, Y., Saint Cloment, C., and Robert, B. (2011). Msx1 and Msx2 in limb mesenchyme modulate digit number and identity. Dev. Dynam. *240*, 1190–1202. https://doi.org/10.1002/dvdy.22619.

Bernal, A., and Arranz, L. (2018). Nestin-expressing progenitor cells: function, identity and therapeutic implications. Cell. Mol. Life Sci. *75*, 2177–2195. https://doi.org/10.1007/s00018-018-2794-z.

Bi, W., Deng, J.M., Zhang, Z., Behringer, R.R., and de Crombrugghe, B. (1999). Sox9 is required for cartilage formation. Nat. Genet. *22*, 85–89. https://doi.org/10.1038/8792.

Carr, M.J., and Johnston, A.P. (2017). Schwann cells as drivers of tissue repair and regeneration. Curr. Opin. Neurobiol. *47*, 52–57. https://doi.org/10.1016/j.conb.2017.09.003.

Chijimatsu, R., and Saito, T. (2019). Mechanisms of synovial joint and articular cartilage development. Cell. Mol. Life Sci. *76*, 3939–3952. https://doi.org/10.1007/s00018-019-03191-5.

Cieza, A., Causey, K., Kamenov, K., Hanson, S.W., Chatterji, S., and Vos, T. (2021). Global estimates of the need for rehabilitation based on the Global Burden of Disease study 2019: a systematic analysis for the Global Burden of Disease Study 2019. Lancet *396*, 2006–2017. https://doi.org/10.1016/s0140-6736(20)32340-0.

Dash, S., and Trainor, P.A. (2020). The development, patterning and evolution of neural crest cell differentiation into cartilage and bone. Bone *137*, 115409. https://doi.org/10.1016/j.bone.2020.115409.

Fitzgerald, J., Rich, C., Burkhardt, D., Allen, J., Herzka, A.S., and Little, C.B. (2008). Evidence for articular cartilage regeneration in MRL/MpJ mice. Osteoarthritis Cartilage *16*, 1319–1326. https://doi.org/10.1016/j.joca.2008.03.014.

Franceschi, R.T., and Xiao, G. (2003). Regulation of the osteoblast-specific transcription factor, Runx2: responsiveness to multiple signal transduction pathways. J. Cell. Biochem. *88*, 446–454. https://doi.org/10.1002/jcb.10369.

Harris, J.D., Siston, R.A., Pan, X., and Flanigan, D.C. (2010). Autologous chondrocyte implantation: a systematic review. J. Bone Joint Surg. Am. *92*, 2220–2233. https://doi.org/10.2106/jbjs.J.00049.

He, J., Yan, J., Wang, J., Zhao, L., Xin, Q., Zeng, Y., Sun, Y., Zhang, H., Bai, Z., Li, Z., et al. (2021). Dissecting human embryonic skeletal stem cell ontogeny by single-cell transcriptomic and functional analyses. Cell Res. *31*, 742–757. https://doi.org/10.1038/s41422-021-00467-z.

Hojo, H., Ohba, S., He, X., Lai, L.P., and McMahon, A.P. (2016). Sp7/Osterix Is Restricted to Bone-Forming Vertebrates where It Acts as a Dlx Co-factor in Osteoblast Specification. Dev. Cell *37*, 238–253. https://doi.org/10.1016/j.devcel.2016.04.002.

Hu, H., Duan, Y., Wang, K., Fu, H., Liao, Y., Wang, T., Zhang, Z., Kang, F., Zhang, B., Zhang, H., et al. (2022). Dental niche cells directly contribute to tooth reconstitution and morphogenesis. Cell Rep. *41*, 111737. https://doi.org/10.1016/j.celrep.2022.111737.

Huangfu, D., Osafune, K., Maehr, R., Guo, W., Eijkelenboom, A., Chen, S., Muhlestein, W., and Melton, D.A. (2008). Induction of pluripotent stem cells from primary human fibroblasts with only Oct4 and Sox2. Nat. Biotechnol. *26*, 1269–1275. https://doi.org/10.1038/nbt.1502.

Humphreys, P.A., Mancini, F.E., Ferreira, M.J.S., Woods, S., Ogene, L., and Kimber, S.J. (2022). Developmental principles informing human pluripotent stem cell differentiation to cartilage and bone. Semin. Cell Dev. Biol. *127*, 17–36. https://doi.org/10.1016/j.semcdb.2021.11.024.

Hunter, D.J., March, L., and Chew, M. (2020). Osteoarthritis in 2020 and beyond: a Lancet Commission. Lancet *396*, 1711–1712. https://doi.org/10.1016/s0140-6736(20)32230-3.

Jin, S., Guerrero-Juarez, C.F., Zhang, L., Chang, I., Ramos, R., Kuan, C.H., Myung, P., Plikus, M.V., and Nie, Q. (2021). Inference and analysis of cell-cell communication using CellChat. Nat. Commun. *12*, 1088. https://doi.org/10.1038/s41467-021-21246-9.

Katz, J.N., Arant, K.R., and Loeser, R.F. (2021). Diagnosis and Treatment of Hip and Knee Osteoarthritis: A Review. JAMA *325*, 568–578. https://doi.org/10.1001/jama.2020.22171.

Koh, Y.G., Choi, Y.J., Kwon, O.R., and Kim, Y.S. (2014). Second-Look Arthroscopic Evaluation of Cartilage Lesions After Mesenchymal Stem Cell Implantation in Osteoarthritic Knees. Am. J. Sports Med. *42*, 1628–1637. https://doi.org/10.1177/0363546514529641.

Kwon, H., Brown, W.E., Lee, C.A., Wang, D., Paschos, N., Hu, J.C., and Athanasiou, K.A. (2019). Surgical and tissue engineering strategies for articular cartilage and meniscus repair. Nat. Rev. Rheumatol. *15*, 550–570. https://doi.org/10.1038/s41584-019-0255-1.

Lallemand, Y., Nicola, M.-A., Ramos, C., Bach, A., Cloment, C.S., and Robert, B. (2005). Analysis of Msx1; Msx2 double mutants reveals multiple roles for Msx genes in limb development. Development *132*, 3003–3014. https://doi.org/10.1242/dev.01877.

Le, H., Xu, W., Zhuang, X., Chang, F., Wang, Y., and Ding, J. (2020). Mesenchymal stem cells for cartilage regeneration. J. Tissue Eng. *11*, 2041731420943839. https://doi.org/10.1177/2041731420943839.

Lefebvre, V., Huang, W., Harley, V.R., Goodfellow, P.N., and de Crombrugghe, B. (1997). SOX9 is a potent activator of the chondrocyte-specific enhancer of the pro alpha1(II) collagen gene. Mol. Cell Biol. *17*, 2336–2346. https://doi.org/10.1128/mcb.17.4.2336.

Lehoczky, J.A., Robert, B., and Tabin, C.J. (2011). Mouse digit tip regeneration is mediated by fate-restricted progenitor cells. Proc. Natl. Acad. Sci. USA *108*, 20609–20614. https://doi.org/10.1073/pnas.1118017108.

Liu, J.A., and Cheung, M. (2016). Neural crest stem cells and their potential therapeutic applications. Dev. Biol. *419*, 199–216. https://doi.org/10.1016/j.ydbio.2016.09.006.

Liu, T.P., Ha, P., Xiao, C.Y., Kim, S.Y., Jensen, A.R., Easley, J., Yao, Q., and Zhang, X. (2022). Updates on mesenchymal stem cell therapies for articular cartilage regeneration in large animal models. Front. Cell Dev. Biol. *10*, 982199. https://doi.org/10.3389/fcell.2022.982199.

Long, H., Zeng, X., Liu, Q., Wang, H., Vos, T., Hou, Y., Lin, C., Qiu, Y., Wang, K., Xing, D., et al. (2020). Burden of osteoarthritis in China, 1990–2017: findings from the Global Burden of Disease Study 2017. Lancet. Rheumatol. *2*, e164–e172. https://doi.org/10.1016/S2665-9913(19)30145-6.

Madeira, C., Santhagunam, A., Salgueiro, J.B., and Cabral, J.M.S. (2015). Advanced cell therapies for articular cartilage regeneration. Trends Biotechnol. *33*, 35–42. https://doi.org/10.1016/j.tibtech.2014.11.003.

Makris, E.A., Gomoll, A.H., Malizos, K.N., Hu, J.C., and Athanasiou, K.A. (2015). Repair and tissue engineering techniques for articular cartilage. Nat. Rev. Rheumatol. *11*, 21–34. https://doi.org/10.1038/nrrheum.2014.157.

Markman, S., Zada, M., David, E., Giladi, A., Amit, I., and Zelzer, E. (2023). A single-cell census of mouse limb development identifies complex spatiotemporal dynamics of skeleton formation. Dev. Cell *58*, 565–581.e4. https://doi.org/10.1016/j.devcel.2023.02.013.

McGonagle, D., Baboolal, T.G., and Jones, E. (2017). Native joint-resident mesenchymal stem cells for cartilage repair in osteoarthritis. Nat. Rev. Rheumatol. *13*, 719–730. https://doi.org/10.1038/nrrheum.2017.182.

McQueen, C., and Towers, M. (2020). Establishing the pattern of the vertebrate limb. Development *147*, dev177956. https://doi.org/10.1242/dev.177956.

Murphy, M.P., Koepke, L.S., Lopez, M.T., Tong, X., Ambrosi, T.H., Gulati, G.S., Marecic, O., Wang, Y., Ransom, R.C., Hoover, M.Y., et al. (2020). Articular cartilage regeneration by activated skeletal stem cells. Nat. Med. *26*, 1583–1592. https://doi.org/10.1038/s41591-020-1013-2.

Ono, N., Balani, D.H., and Kronenberg, H.M. (2019). Chapter One - Stem and progenitor cells in skeletal development. In Current Topics in Developmental Biology, B.R. Olsen, ed. (Academic Press), pp. 1–24. https://doi.org/10.1016/bs.ctdb.2019.01.006.

Prummel, K.D., Nieuwenhuize, S., and Mosimann, C. (2020). The lateral plate mesoderm. Development *147*, dev175059. https://doi.org/10.1242/dev.175059.

Ranganath, P., Perala, S., Nair, L., Pamu, P.K., Shankar, A., Murugan, S., and Dalal, A. (2020). A newly recognized multiple malformation syndrome with caudal regression associated with a biallelic

c.402G>A variant in TBX4. Eur. J. Hum. Genet. *28*, 669–673. https://doi.org/10.1038/s41431-020-0572-5.

Royle, S.R., Tabin, C.J., and Young, J.J. (2021). Limb positioning and initiation: An evolutionary context of pattern and formation. Dev. Dynam. *250*, 1264–1279. https://doi.org/10.1002/dvdy.308.

Serowoky, M.A., Arata, C.E., Crump, J.G., and Mariani, F.V. (2020). Skeletal stem cells: insights into maintaining and regenerating the skeleton. Development *147*, dev179325. https://doi.org/10.1242/dev.179325.

Steadman, J.R., Briggs, K.K., Rodrigo, J.J., Kocher, M.S., Gill, T.J., and Rodkey, W.G. (2003). Outcomes of microfracture for traumatic chondral defects of the knee: Average 11-year follow-up. Arthroscopy *19*, 477–484. https://doi.org/10.1053/jars.2003.50112.

Street, K., Risso, D., Fletcher, R.B., Das, D., Ngai, J., Yosef, N., Purdom, E., and Dudoit, S. (2018). Slingshot: cell lineage and pseudotime inference for single-cell transcriptomics. BMC Genom. *19*, 477. https://doi.org/10.1186/s12864-018-4772-0.

Tokoyoda, K., Hauser, A.E., Nakayama, T., and Radbruch, A. (2010). Organization of immunological memory by bone marrow stroma. Nat. Rev. Immunol. *10*, 193–200. https://doi.org/10.1038/nri2727.

Wilson, A., and Trumpp, A. (2006). Bone-marrow haematopoietic-stem-cell niches. Nat. Rev. Immunol. *6*, 93–106. https://doi.org/10.1038/nri1779.

Xi, H., Langerman, J., Sabri, S., Chien, P., Young, C.S., Younesi, S., Hicks, M., Gonzalez, K., Fujiwara, W., Marzi, J., et al. (2020). A Human Skeletal Muscle Atlas Identifies the Trajectories of Stem and Progenitor Cells across Development and from Human Pluripotent Stem Cells. Cell Stem Cell *27*, 158–176.e10. https://doi.org/10.1016/j.stem.2020.04.017.

Yamada, D., Nakamura, M., Takao, T., Takihira, S., Yoshida, A., Kawai, S., Miura, A., Ming, L., Yoshitomi, H., Gozu, M., et al. (2021). Induction and expansion of human PRRX1+ limb-bud-like mesenchymal cells from pluripotent stem cells. Nat. Biomed. Eng. *5*, 926–940. https://doi.org/10.1038/s41551-021-00778-x.

Zhu, H., Guo, Z.K., Jiang, X.X., Li, H., Wang, X.Y., Yao, H.Y., Zhang, Y., and Mao, N. (2010). A protocol for isolation and culture of mesenchymal stem cells from mouse compact bone. Nat. Protoc. *5*, 550–560. https://doi.org/10.1038/nprot.2009.238.

Stem Cell Reports, Volume *19*

Supplemental Information

MSX1^{+}PDGFRA^{low} limb mesenchyme-like cells as an efficient stem cell source for human cartilage regeneration

Yuansong Liao, Fanchen Kang, Jingfei Xiong, Kun Xie, Mingxu Li, Ling Yu, Yuqing Wang, Hanyi Chen, Guogen Ye, Yike Yin, Weihua Guo, Haoyang Cai, Qing Zhu, and Zhonghan Li

Supplemental Figures

Figure S1

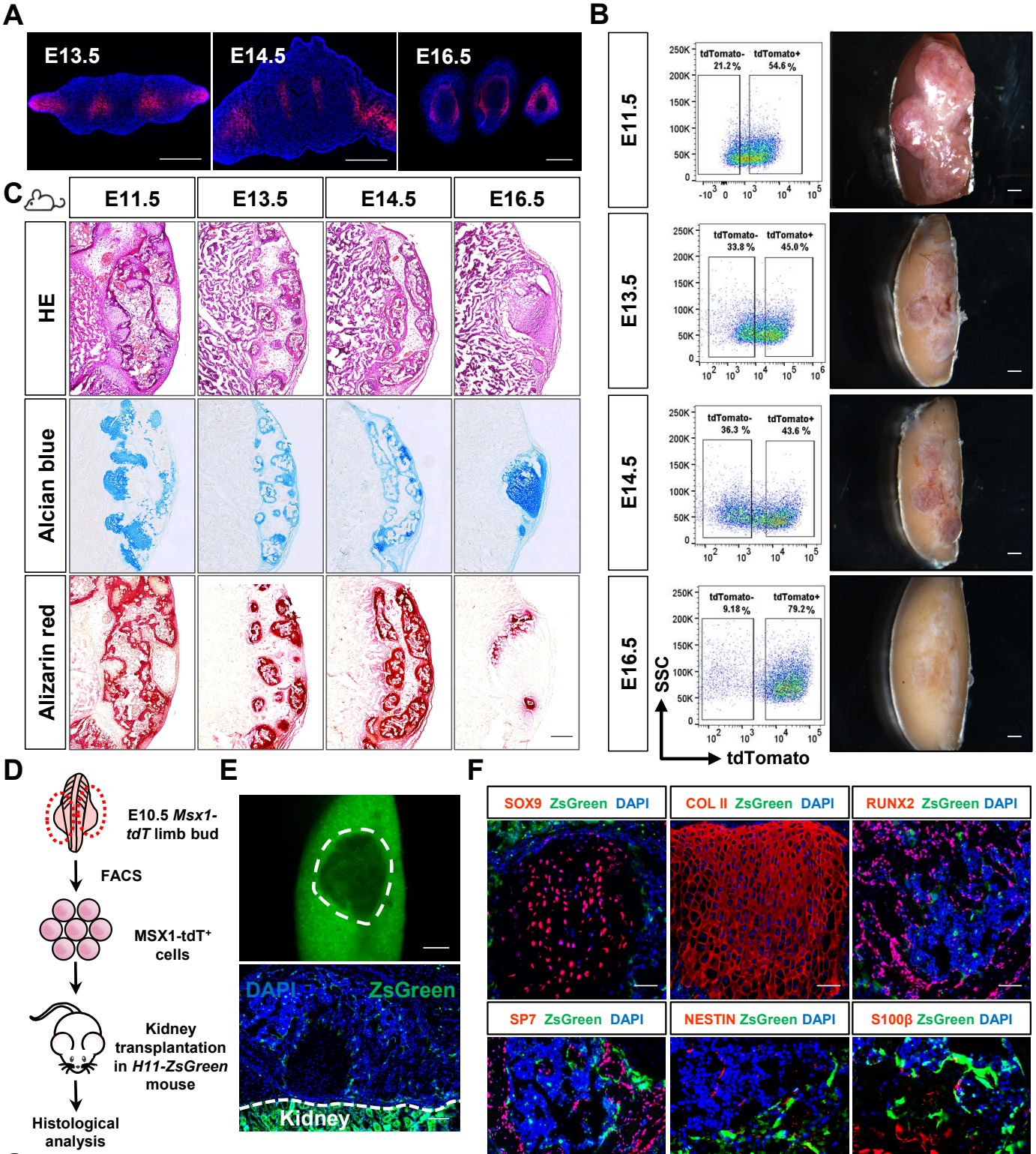

Figure S1. Primary limb bud-derived MSX1$^+$ mesenchymal progenitors exhibited strong bone regenerative capability. (A) Longitudinal sections of the hind limb at E13.5/E14.5/E16.5 stages. The expression of MSX1 was located in the interdigital regions. Scale bars: 200 μm. (B) MSX1$^+$ cells isolated from the selected stages could form bone-like tissues under the kidney capsule. Left: isolation of primary MSX1$^+$ progenitors by cell sorting; Right: representative images of the bone-like tissues formed by the sorted MSX1$^+$ progenitors from the corresponding stages. Scale bars: 1 mm. (C) Histology analysis of bone-like tissues formed by E11.5, E13.5, E14.5, and E16.5 MSX1$^+$ cells. Representative images of HE, Alcian blue, and alizarin red staining were shown. Scale bars: 250 μm. (D) Schematic illustration of MSX1$^+$ cell transplantation in the ZsGreen recipient mice. MSX1$^+$ cells were transplanted in a ZsGreen-expressing host to verify the cell origin of regenerated bone-like tissues. (E) Immunofluorescence images showing bone-like tissues were ZsGreen negative. Scale bars: 1 mm (top), 100 μm (bottom). (F-G) Immunostaining and quantitative analysis of different cell lineages within the transplants. Almost all chondrocytes, osteocytes, and most of the neural and VECs were derived from the transplanted limb MSX1$^+$ mesenchymal progenitors. Scale bars: 50 μm. Error bars represented data from three samples of three independent experiments.

Figure S2

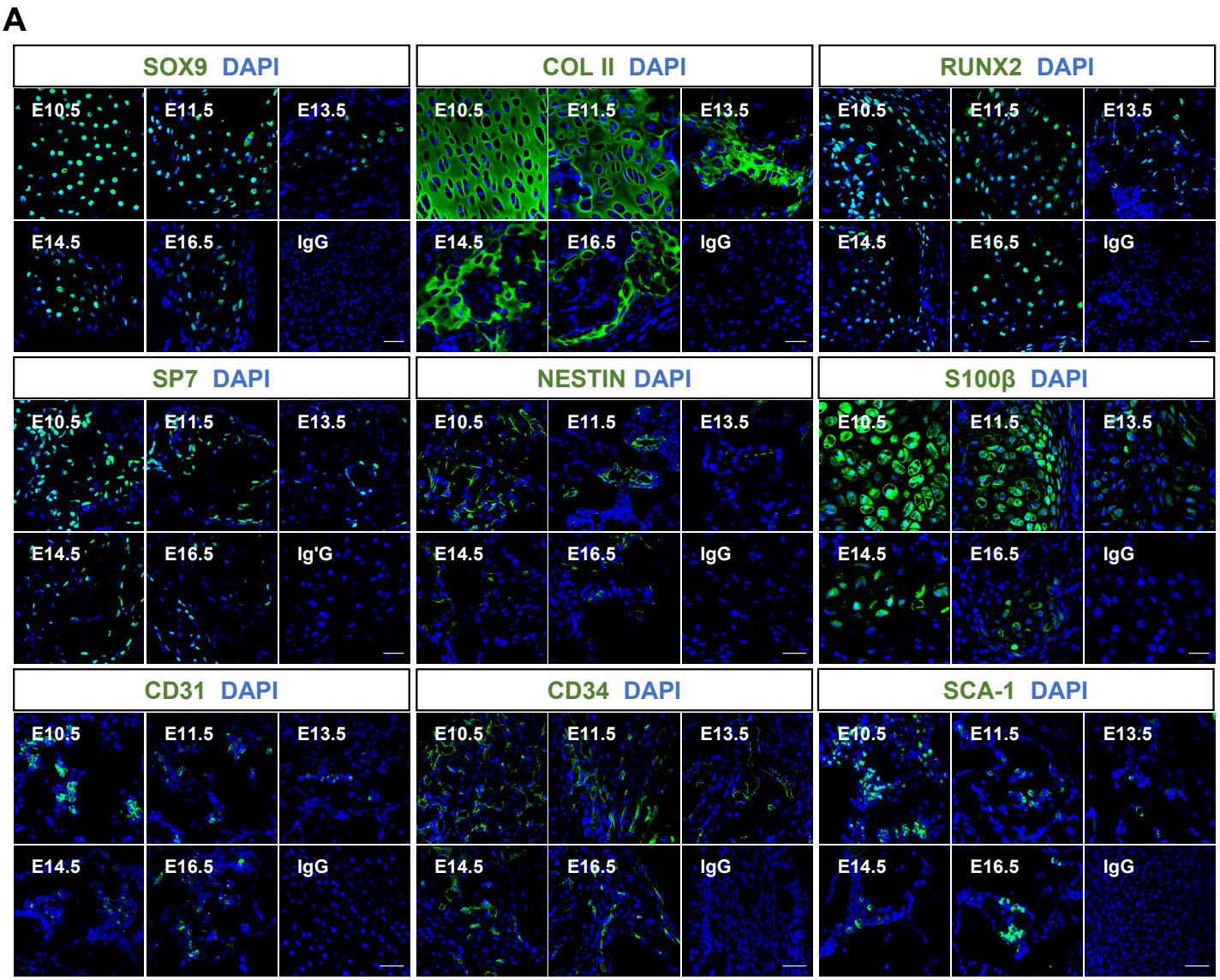
A
SOX9 DAPI
COL II DAPI
RUNX2 DAPI
SP7 DAPI
NESTIN DAPI
S100β DAPI
CD31 DAPI
CD34 DAPI
SCA-1 DAPI
E10.5
E11.5
E13.5
E14.5
E16.5
IgG
B
Area fraction of SOX9/DAPI(%)
Area fraction of COL II/DAPI(%)
Area fraction of RUNX2/DAPI(%)
Area fraction of SP7/DAPI(%)
Area fraction of NESTIN/DAPI(%)
Area fraction of S100β/DAPI(%)
Area fraction of CD31/DAPI(%)
Area fraction of CD34/DAPI(%)
Area fraction of SCA-1/DAPI(%)

Figure S2. E10.5 limb bud MSX1^{+} mesenchymal progenitors exhibited strong bone regenerative capability. (A) Immunostaining characterization of osteochondral markers in the regenerated bone-like tissues using MSX1^{+} cells from different developmental stages. The markers were the same as in Figure 1F. Scale bars: 25 μm (SOX9, COL II, RUNX2, and SP7) and 30 μm (NESTIN, S100β, CD31, CD34, and SCA-1). (B) Quantitative analysis of osteochondral markers in regenerated bone-like tissues. The results confirmed that E10.5 MSX1^{+} cells had the most efficient regenerative potential. Error bars represented data from fifteen sections of three independent transplantation experiments (with at least three transplants for each group, mean ± SD). Statistical significance was marked as different letters. Different letters between the two groups indicated statistical significance while possessing the same letter indicated otherwise. Statistics: One-way ANOVA followed by Tukey (CD34) and Tamhane's T2 (SOX9, COL II, RUNX2, SP7, NESTIN, S100β, CD31, and SCA-1) post hoc multiple comparisons by SPSS v22.0.

Figure S3

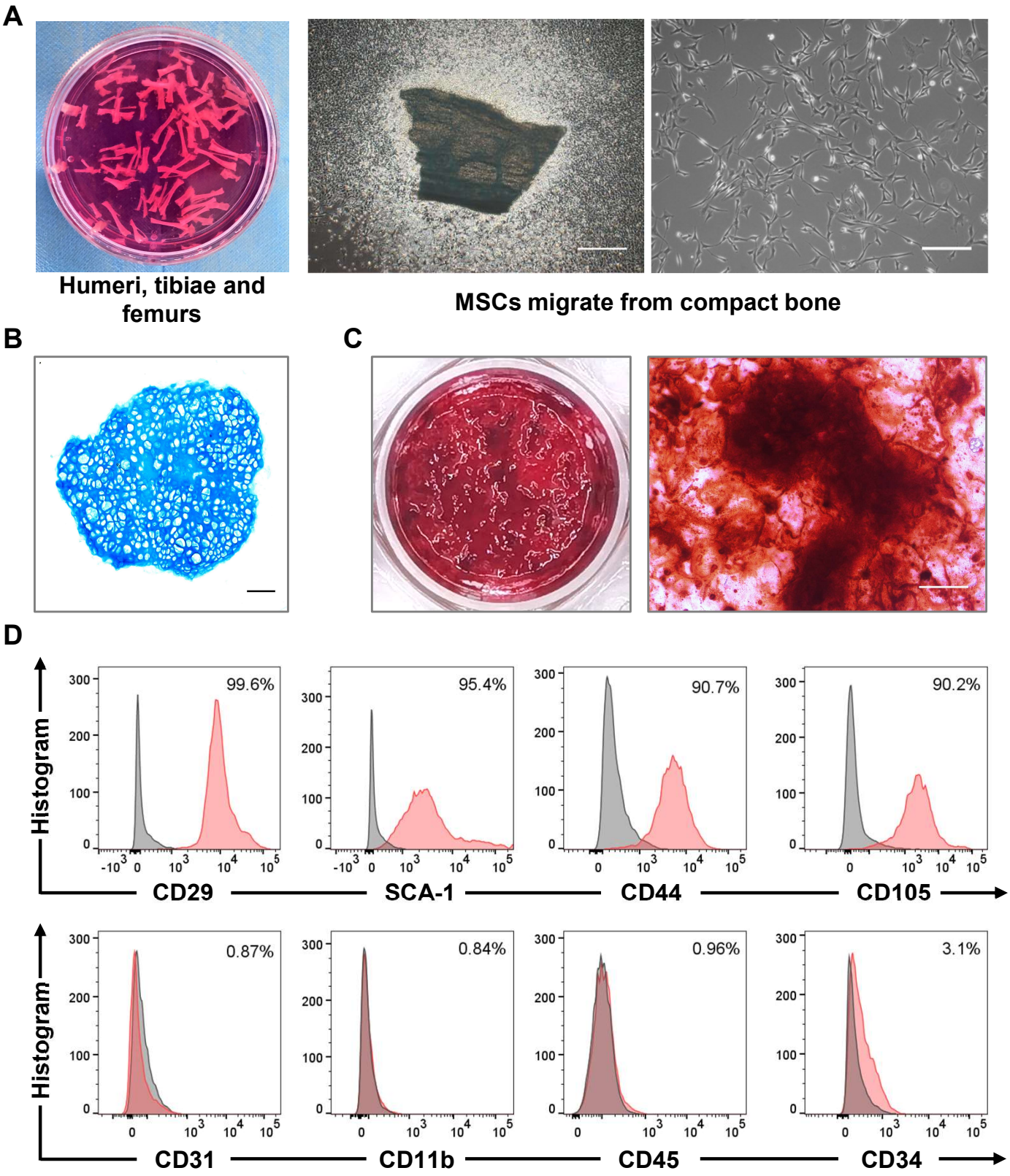

Figure S3. The isolation and characterization of MSCs from murine compact bones. (A) Isolation and culture of MSCs from the compact bones. Left: isolated mouse compact bones. Middle: MSCs migrated out from the bone chips. Right: morphology of isolated MSCs. Scale bars: 500 μm (middle), 100 μm (right). (B-C) Multilineage differentiation of the isolated MSCs. Chondrogenesis was evaluated by Alcian blue (left) and osteogenesis by alizarin red staining (right). Scale bars: 50 μm (left), 100 μm (right). (D) Flow cytometry analysis confirmed the presence of classical MSC markers in the isolated cells. Isolated MSC cells were positive for SCA-1, CD29, CD44, and CD105, but negative for CD11b, CD31, CD34, and CD45.

Figure S4

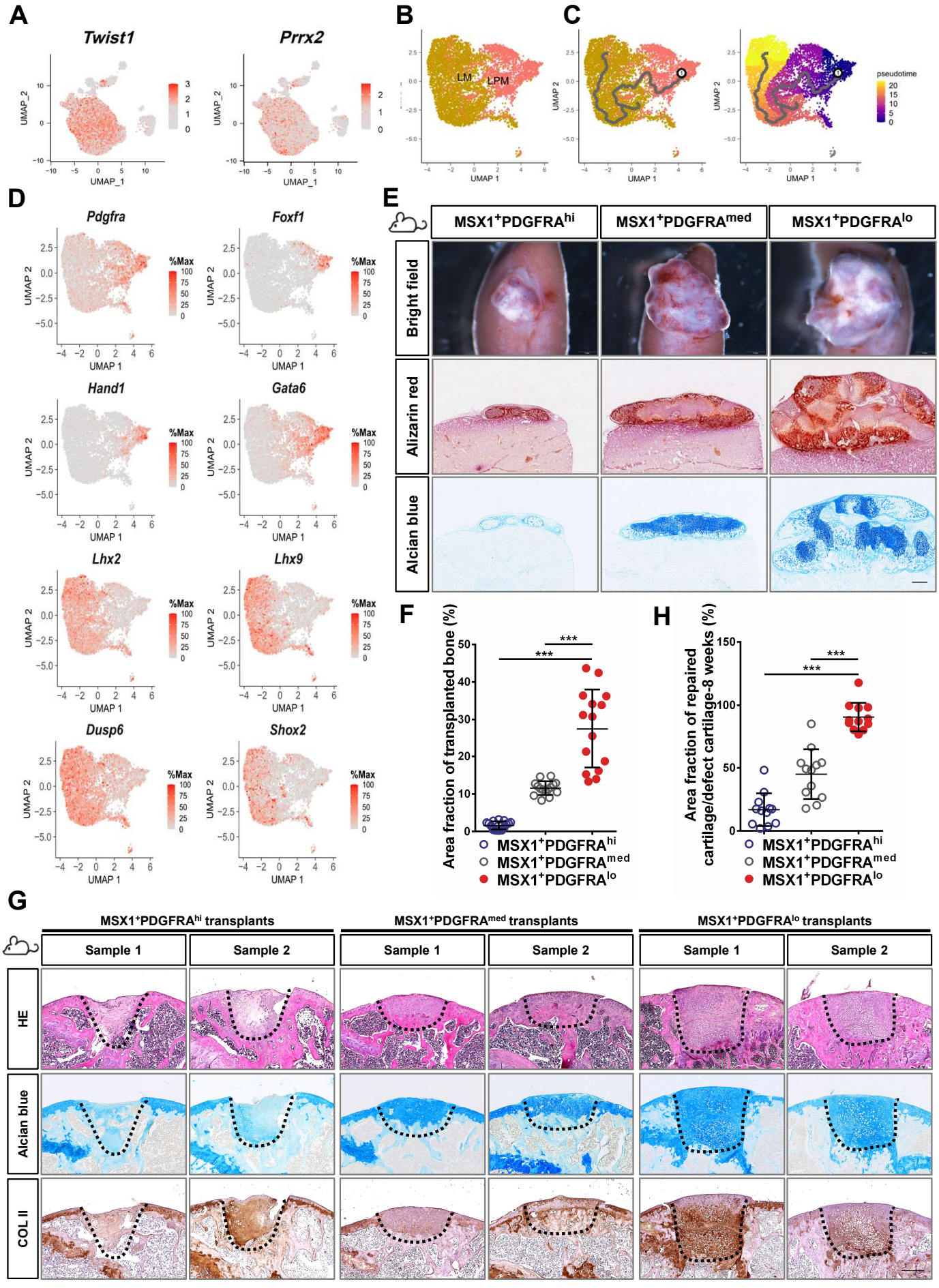
A
Twist1
Prrx2
UMAP_1
UMAP_2
B
LM
LPM
UMAP 1
C
pseudotime
D
Pdgfra
Foxf1
Hand1
Gata6
Lhx2
Lhx9
Dusp6
Shox2
%Max
E
MSX1+PDGFRAhi
MSX1+PDGFRAmed
MSX1+PDGFRAlo
Bright field
Alizarin red
Alcian blue
F
Area fraction of transplanted bone (%)
***
H
Area fraction of repaired cartilage/defect cartilage-8 weeks (%)
G
MSX1+PDGFRAhi transplants
MSX1+PDGFRAmed transplants
MSX1+PDGFRAlo transplants
Sample 1
Sample 2
HE
Alcian blue
COL II

Figure S4. ScRNA-seq analysis identified MSX1^{+}PDGFRA^{low} limb bud cells as the key cell composition with strong bone regenerative capability. (A) Most of the E10.5 MSX1^{+} progenitor cells highly expressed mesenchymal makers *Prrx2* and *Twist1*. (B) UMAP plots of mesenchymal cells exhibited the two major subsets (LPM and LM cells) for downstream trajectory analysis. (C) Pseudotime trajectory analysis identified the LM cells as the descendants of LPM. (D) UMAP plots showing the marker gene expressions for LPM cells (*Pdgfra*$^{+}$ *Foxf1*$^{+}$ *Hand1*$^{+}$ *Gata6*$^{+}$), LM cells (*Lhx2*$^{+}$ *Lhx9*$^{+}$ *Dusp6*$^{+}$ *Shox2*$^{+}$). (E) Confirmation of the bone regeneration capability of MSX1^{+}PDGFRA^{low} cells *in vivo*. The sorted cells were transplanted into the kidney capsule of the recipient mice and analyzed after three weeks. Representative images were shown. Alcian blue staining was used to detect cartilage formation and alizarin red staining for osteogenesis. Scale bars: 1 mm (BF), 500 μm (Alcian blue and alizarin red). (F) Quantitative analysis of bone-like tissues indicated that the MSX1^{+}PDGFRA^{low} cells retained the strongest osteochondral competency among the tested cell populations. Error bars represented data from fifteen sections of three independent experiments with at least three transplants for each group (mean ± SD). Statistics: One-way ANOVA followed by Tamhane's T2 post hoc multiple comparisons by SPSS v22.0. ***p<0.001. (G) Regenerated cartilage by mouse MSX1^{+}PDGFRA^{low} cells could be maintained for at least 8 weeks. Samples were analyzed 8 weeks post-transplantation. The defect sites were filled with hyaline chondrocytes confirmed by Alcian blue and COL II staining. Scale bars: 200 μm. (H) Quantitative analysis revealed MSX1^{+}PDGFRA^{low} cells possessed the highest cartilage regeneration efficiency. Error bars represented data from twelve sections of six mice in three independent experiments (mean ± SD). Statistics: One-way ANOVA followed by Tukey post hoc multiple comparisons by SPSS v22.0. ***p<0.001.

Figure S5

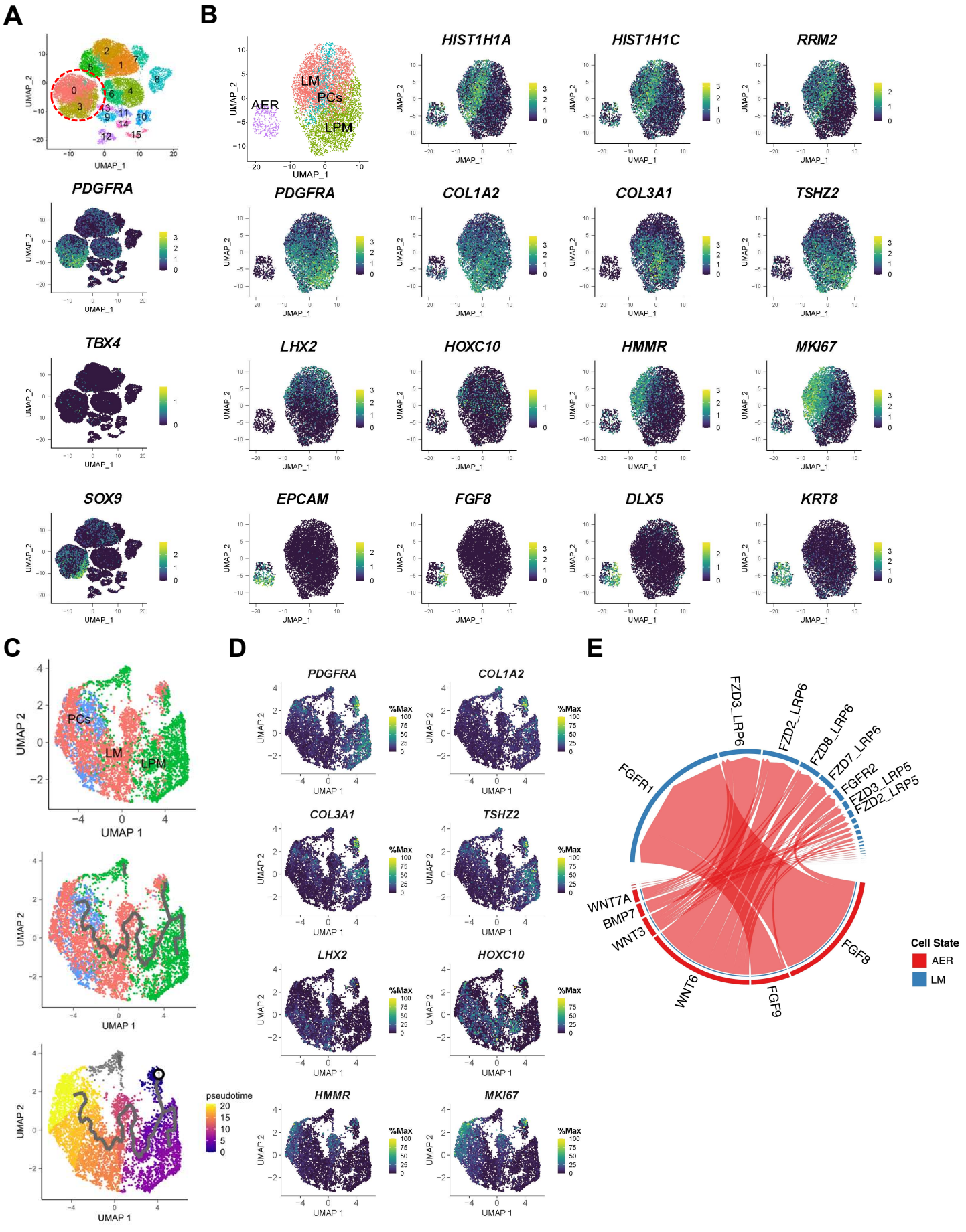
A
B
C
D
E
UMAP_1
UMAP_2
AER
LM
PCs
LPM
HIST1H1A
HIST1H1C
RRM2
PDGFRA
COL1A2
COL3A1
TSHZ2
TBX4
LHX2
HOXC10
HMMR
MKI67
SOX9
EPCAM
FGF8
DLX5
KRT8
UMAP 1
UMAP 2
pseudotime
%Max
FZD3_LRP6
FZD2_LRP6
FZD8_LRP6
FZD7_LRP6
FGFR2
FZD3_LRP5
FZD2_LRP5
FGFR1
WNT7A
BMP7
WNT3
WNT6
FGF9
FGF8
Cell State
AER
LM

Figure S5. ScRNA-seq analysis of 5 WPC human limbs. (A) UMAP plots of gene expression profiles for primary human limb bud cells at 5 WPC identified 16 cell clusters. Based on the expression of *PDGFRA*, *TBX4*, and *SOX9*, clusters 0 and 3 were considered to be hindlimb cells (red dashed line). (B) Together with the identified hindlimb cells, human AER (cluster 10 in Figure S5A) was also isolated for downstream Cellchat analysis. UMAP plots of clusters 0, 3, and 10 were colored by cell type, including LM (red), LPM (green), PCs (proliferating cells of LPM and LM, blue), and AER (purple). The expressions of different marker genes in selected clusters were listed. PCs: *HIST1H1A*, *HIST1H1C*, *RRM2*. LPM: *PDGFRA*, *COL1A2*, *COL3A1*, *TSHZ2*. LM: *LHX2*, *HOXC10*, *HMMR*, *MKI67*. AER: *EPCAM*, *FGF8*, *DLX5*, *KRT8*. (C) Pseudotime differentiation trajectory analysis projected that human hindlimb cells sequentially undergo differentiation from LPM to LM. PCs: proliferating cells. (D) UMAP plots showing the expression of specific marker genes along the trajectory from human LPM (*PDGFRA*$^+$ *COL1A2*$^+$ *COL3A1*$^+$ *TSHZ2*$^+$), to human LM cells (*LHX2*$^+$ *HOXC10*$^+$ *HMMR*$^+$ *MKI67*$^+$). (E) Analysis of potential ligands and receptors by Cellchat to drive LM development. The results indicated that most of the candidates were enriched in WNT and FGF signaling pathways.

Figure S6

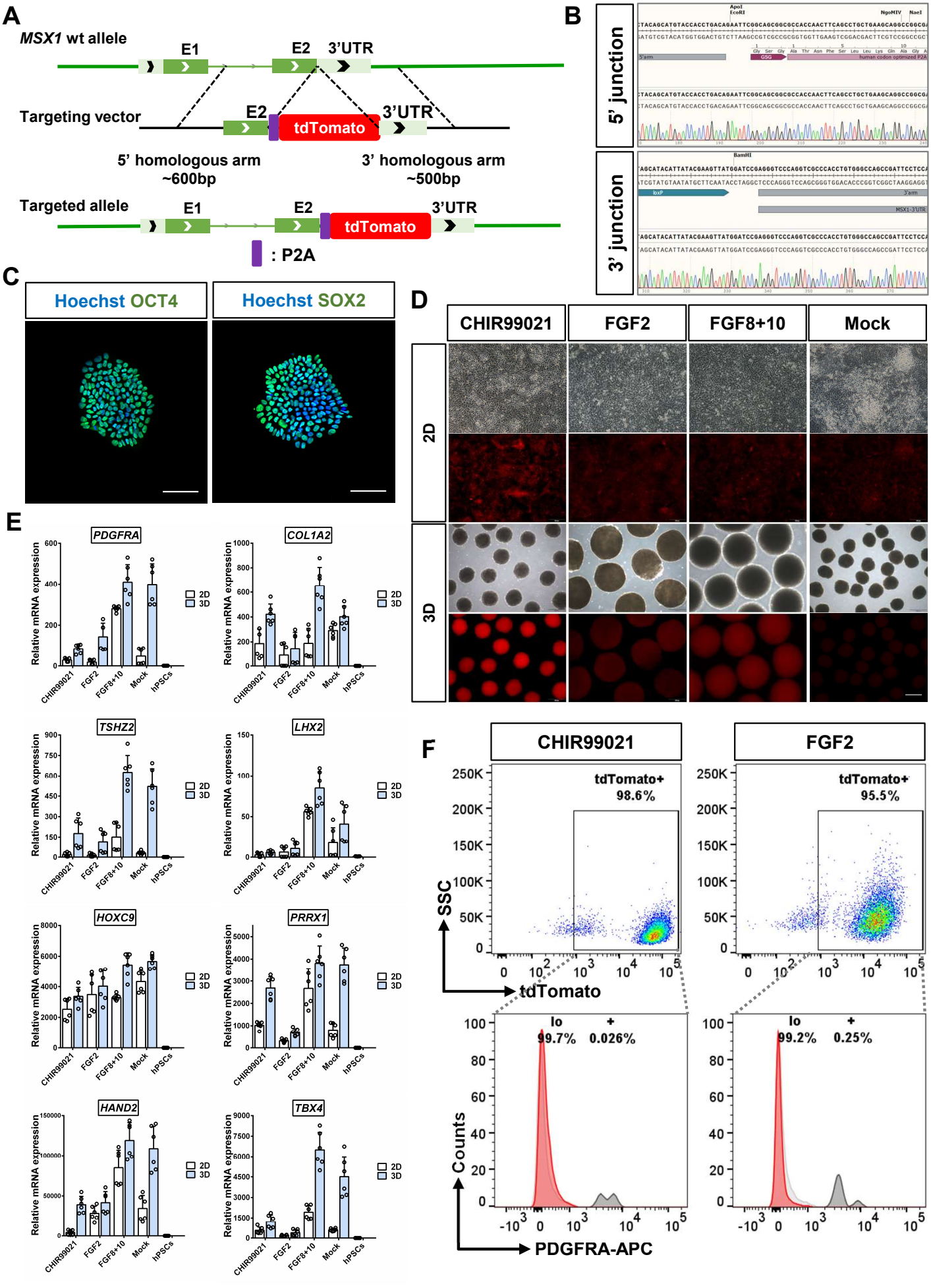
A
MSX1 wt allele
E1
E2
3'UTR
Targeting vector
E2
tdTomato
3'UTR
5' homologous arm
~600bp
3' homologous arm
~500bp
Targeted allele
E1
E2
tdTomato
3'UTR
: P2A
B
5' junction
3' junction
C
Hoechst OCT4
Hoechst SOX2
D
CHIR99021
FGF2
FGF8+10
Mock
2D
3D
E
PDGFRA
COL1A2
TSHZ2
LHX2
HOXC9
PRRX1
HAND2
TBX4
Relative mRNA expression
2D
3D
CHIR99021
FGF2
FGF8+10
Mock
hPSCs
F
CHIR99021
FGF2
tdTomato+
98.6%
tdTomato+
95.5%
SSC
tdTomato
Counts
lo
+
99.7%
0.026%
lo
+
99.2%
0.25%
PDGFRA-APC

Figure S6. Generation of the *MSX1*$^{P2A\text{-}tdTomato}$ knock-in cell line induction of LM-like cells in hPSCs. (A) Schematic procedure of cell line construction. A P2A-tdTomato cassette was inserted into the human *MSX1* loci by homologous recombination. (B) The P2A-tdTomato cassette was inserted into the loci behind exon2 of human *MSX1* by the HDR-based CRISPR/Cas9 method, confirmed by genome sequencing. (C) Immunostaining of SOX2 and OCT4 confirmed pluripotency of the knock-in cells. Scale bars: 75 μm. (D) Bright-field and fluorescent microscopy of day 8 MSX1^{+} (tdTomato^{+}) cells following different treatments with small molecules and growth factors under 2D and 3D conditions. Scale bars: 500 μm. (E) qRT-PCR analysis revealed LM marker gene expressions were significantly enriched in FGF8+10 treated cells, especially in the 3D culture. LPM makers: *PDGFRA*, *COL1A2* and *TSHZ2*. LM makers: *LHX2* and *HOXC9*. Mesenchymal markers: *HAND2* and *PRRX1*. Hindlimb-specific marker: *TBX4*. Error bars represented data from two independent experiments with duplicates. Each sample contained three technique replicates. (F) FACS sorting of the CHIR99021 and FGF2 treated groups by tdTomato (MSX1) and PDGFRA.

Supplemental Tables

Table S1. List of primary antibodies used for immunostaining, related to Supplemental experimental procedures

Target	Antibody Name	Vendor	Catalog Number
Mouse CD29/ CD105/CD44/CD45/ SCA-1/CD11b	Anti-CD29/ CD105/CD44/CD45/ SCA-1/CD11b antibodies	R&D systems	SC018
Mouse CD31	Anti-CD31 antibody	Invitrogen	11-0311-82
Mouse CD34	Anti-CD34 antibody	Invitrogen	11-5981-82
Mouse PDGFRA	anti-PDGFRA antibody	Biolegend	135907
Mouse SOX9	anti-SOX9 antibody	HUABIO	ET1611-56
Mouse COL II	anti-COL II antibody	Invitrogen	MA5-12789
Mouse SP7	Anti-SP7 antibody	Abcam	ab209484
Mouse RUNX2	anti-RUNX2 antibody	HUABIO	ET1612-47
Mouse NEATIN	anti-NESTIN antibody	HUABIO	R1510-19
Mouse S100β	anti-S100β antibody	HUABIO	ET1610-3
Mouse CD34	anti-CD34 antibody	HUABIO	ET606-11
Mouse SCA-1	anti-SCA-1 antibody	Invitrogen	11-5981-82
Human OCT4	anti-OCT4 antibody	Abcam	ab19857
Human SOX2	anti-SOX2 antibody	Abcam	ab97959
Human PDGFRA	anti-PDGFRA antibody	Biolegend	323512

Table S2. Primers used in genome sequencing of Msx1$^{P2A\text{-}tdTomato}$ knock-in hPSCs cell line, related to Result and Experimental procedures sections.

Targets	Direction	Sequence (5'-3')
Msx1-5'	Forward	CACATCTTCCCAGCTGTTTAGGCC
Msx1-3'	Reverse	CCTACCTTTGCAACACATCTGTGTTTTCC
tdTomato-1	Reverse	GAACTCTTTGATGACGGCCATGTTG
tdTomato-2	Forward	CCTCCGAGGACAACAACATGGCC
PGK-1	Reverse	CCATTTGTCACGTCCTGCACGAC
PGK-2	Forward	GCCTCGCACACATTCCACATCCA
Puro-1	Reverse	GGCTTGCGGGTCATGCACCA
Puro-2	Forward	CTTCTACGAGCGGCTCGGCTTCA

Table S3. Primers of qRT-PCR used in this article were listed, related to Result and Experimental procedures sections.

Targets	Direction	Sequence (5'-3')
GAPDH	Forward	TGCCAAATATGATGACATCAAGAA
	Reverse	GGAGTGGGTGTCGCTGTTG
PDGFRA	Forward	GATTGTGGTCACCTGTGCTG
	Reverse	TCTTCCAGCATTGTGATGCC
COL1A2	Forward	GAGGACCACGTGGAGAAAGG
	Reverse	CAAAGTTCCCACCGAGACCA
COL3A1	Forward	GCTACTTCTCGCTCTGCTTC
	Reverse	CCGCATAGGACTGACCAAGA
TSHZ2	Forward	CCACCCACATGATGGTCACA
	Reverse	GCTTGGGAGCCAGAGAATCA
LHX2	Forward	GGACGGTAGCATCTACTGCAA
	Reverse	CCCGTGGTCAGCATCTTGTT
HOXC10	Forward	AAAGGAGAGGGCCAAAGCTG
	Reverse	TTCCTTCCGCTCTTTGCTGT
HMMR	Forward	GGCTGGTCAAGCAATTGGAA
	Reverse	CCTGGGTATGAGCAGCACTA
MKI67	Forward	ACACTCCACCTGTCCTGAAG
	Reverse	CCAAGCTTTGTGCCTTCACT
HOXC9	Forward	GCAGCAAGCACAAAGAGGAG
	Reverse	CAGCGTCTGGTACTTGGTGT
TBX4	Forward	TCCAGAAGCTGAAGCTGACA
	Reverse	GGAGCCGAAAGCATTGTTCT
Gapdh	Forward	GCACAGTCAAGGCCGAGAAT
	Reverse	GCCTTCTCCATGGTGGTGAA
Pdgfra	Forward	AGGCAGGGCTTCAACGGAAC
	Reverse	AAGACGGCACAGGTCACCAC
Foxf1	Forward	CTGGAGCAGCCATACCTTCA
	Reverse	TGAGTGATACCGAGGGATGC
Hand1	Forward	TGGCCAAGGATGCACAAGCA
	Reverse	AAGCTTTCGGGCTGCTGAGG
Isl1	Forward	TGGAGACCCTCTCAGTCCCT
	Reverse	AGCTGCTTCTCGTTGAGCAC
Lhx2	Forward	CTTCAGCAAGGATGGCAGCA
	Reverse	GCGCATCACCATCTCTGAGG
Lhx9	Forward	CCAGCTCTGGGAGTGGACAT
	Reverse	CCAAGTGGTCTGCCTCGTTC

Supplemental experimental procedures

Mouse strains and animal care

All animal experiments were approved by the Institutional Animal Care and Use Committee at the College of Life Sciences, Sichuan University. All animals were maintained under standardized conditions with the temperature- and light-controlled (25 °C, 12 h light/dark cycle), in individually ventilated cages, and had free access to food and water. Knock-in C57BL6-*Msx1*$^{P2A\text{-}tdTomato}$ mice and *H11-ZsGreen* mice were custom-generated by Biocytogen, Inc. (Beijing). Mouse offspring from these strains were routinely genotyped using standard PCR protocols. C57BL6 wt mice and NOD-SCID mice were purchased from Gempharmatech Co., Ltd (Chengdu). C57BL6 wt mice were used as recipients for renal subcapsular and articular cartilage transplantation of mouse MSX1$^+$ cells, while NOD-SCID mice were used as recipients for articular cartilage transplantation of differentiated human LPM- and LM-like cells.

Flow cytometry

Primary mouse MSX1$^+$ (tdTomato$^+$) cells were sorted by BD FACS Aria II (BD Biosciences, USA). To identify the surface markers, compact bone derived-MSCs were stained with anti-CD29/CD105/CD44/CD45/SCA-1/CD11b (R&D systems, Cat# SC018), CD31 (Invitrogen, Cat# 11-0311-

82), CD34 (Invitrogen, Cat# 11-5981-82) antibodies at 4 °C for 30 min. After washing in phosphate-buffered saline (PBS) (3 × 5 min), secondary antibodies were incubated for 30 min at room temperature (except for CD31 and CD34 staining). These cells were suspended in FACS sorting buffer after washing them in PBS (3 × 5 min).

Dissociation of mouse hindlimb cells and the differentiated human day 8 cells was performed with 0.25% Trypsin-EDTA (ThermoFisher, Cat# 25200072) at 37 °C for 5 min. Then digestion was terminated by adding a complete medium (DMEM + 15% FBS (Gibco, Cat# 10099–141) + 1% Glutamax + 1% NEAA + 0.1% β-mercaptoethanol + 1% Pen-Strep (Gibco, Cat# 15140122)). After centrifuged at 450 g for 3 min and resuspended in PBS, the collected cells were stained with anti-PDGFRA (Biolegend, Cat# 135907 (for mouse cells); Cat# 323512 (for human cells), 1: 100) antibodies on ice and then prepared in FACS sorting buffer (1 × PBS with 1% bovine serum albumin (BSA (Sigma-Aldrich, Cat# A9418-100G) for subsequent sorting. FlowJo (v10) software was used for analyzing the flow cytometry data.

Renal subcapsular transplantation of mouse MSX1^{+} hindlimb cells

E10.5/E11.5/E13.5/E14.5/E16.5 *Msx1*$^{P2A\text{-}tdTomato}$ hindlimbs were dissected and transferred to PBS. After centrifuging and removing the supernatant, 0.25% Trypsin-EDTA was added to digest these limb buds into single cells.

Following incubation at 37 °C for 5 min, digestion was terminated by adding the complete medium. After centrifugation at 450 g for 3 min, the collected cells were resuspended in the FACS sorting buffer. Flow cytometry was performed on BD FACS Aria II, with wt hindlimb cells being used as a negative control. 1.5×10^5 sorted $MSX1^+$ cells at all stages were embedded in collagen I (Advanced BioMatrix, Cat# P5005) and incubated at 37 °C for 24 h in the complete medium. Before transplantation, clumps of these $MSX1^+$ cells were stripped from the collagen. Then 8-week C57BL6 wt mice were anesthetized by an intraperitoneal injection of Avertin (1.25 g 2, 2, 2-Tribromoethanol (Sigma-Aldrich, Cat# T48402) + 2.5 mL 2-Methyl-2-butanol (Sigma-Aldrich, Cat# 721123) + 97.5 mL UP H_2O) and the skin was disinfected with 75% ethanol. After making a 0.5 cm longitudinal incision in the upper skin and muscle, the kidney was observed and a small incision was made near the kidney pole to separate the capsule from the renal parenchyma (Nakao et al., 2007). Then clumps of $MSX1^+$ cells were transplanted into the kidney capsule under a dissecting microscope. Finally, the mice were placed in sterile cages after the skin was closed with Michel's clamps. Three weeks post-transplantation, grafts were dissected and fixed in 4% paraformaldehyde (PFA) at 4 °C for 24 h and then dehydrated in 30% sucrose at 4 °C for more than 48 h. Grafts were then sectioned under a -20 ℃ condition to get frozen sections and stained by H&E (Solarbio, Cat# G1120-3), Masson (Solarbio,

Cat# G1346), alizarin red (Sigma-Aldrich, Cat# A5533), and Alcian blue (Sigma, Cat# A3157) to demonstrate bone sand cartilage differentiation using manufacturer's protocol.

Articular cartilage repair

The method of isolating compact bone-derived MSCs has been described previously in detail (Zhu et al., 2010). Mouse $MSX1^+$ cells, MSCs, and the differentiated human cells were embedded in collagen I and incubated at 37 ℃ in the corresponding medium (mouse $MSX1^+$ cells were cultured in the complete medium, MSCs were cultured in α-MEM (Gibco, Cat# C12571500BT) containing 10% FBS and 1% Pen-Strep, human day 8 cells were cultured in LM medium) for 24 h before transplantation. Cell aggregates needed to be dissected with part of collagen I before the defect sites were prepared.

8 weeks old C57BL6 male mice were used in the surgery to make cartilage lesions. The transplantation protocols had been described previously in detail (Fitzgerald, Rich, et al. 2008). Briefly, the mice were anesthetized by an intraperitoneal injection of Avertin, the hair was clipped over the right knee, then the skin was disinfected, and the animals were placed under a dissecting microscope. A small (0.5-1 cm) skin incision was made above the patella, then the joint capsule was opened, and the patella was luxated laterally to expose the trochlear groove articular surface. For

the full-thickness lesion, a circular 0.8 mm defect was conducted in the cartilage with a 23G needle using a circular motion until the subchondral bone was reached (or blood appeared flowing removal of the needle). The cell aggregate was then removed into the cartilage defect. The joint capsule was closed with absorbable 8-0 suture and the skin was closed with a 4-0 suture. The mice were allowed to recover in clean, corncob-lined boxes. There was no evidence of mice lameness or systemic effects for the duration of the experiment. Three or eight weeks later, the transplanted femurs were isolated, and histological analysis was followed.

Immunostaining

Before staining, frozen sections (6 μm) of renal transplantation were washed in PBS gently for 3 min. After being treated with antigen retrieval solution (Solarbio, Cat# C1035), permeabilization was conducted with 0.3% PBST (0.3% Triton X-100 in PBS) (except for membrane proteins), followed by blocking with 5% BSA. Then sections were stained with anti-SOX9 (HUABIO, Cat# ET1611-56, 1: 200), COL II (Invitrogen, Cat# MA5-12789, 1: 200), RUNX2 (HUABIO, Cat# ET1612-47, 1: 200), SP7 (Abcam, Cat# ab209484, 1:200), NESTIN (HUABIO, Cat# R1510-19, 1: 200), S100β (HUABIO, Cat# ET1610-3, 1: 200), CD31 (Invitrogen, Cat# 11-0311-82, 1: 200), CD34 (HUABIO, Cat# ET606-11, 1: 200), SCA-1 (Invitrogen, Cat# 11-5981-82, 1: 100) antibodies at 4 °C overnight. After

washing in PBS (3 × 5 min), secondary antibodies were incubated for 1 h at room temperature (except for the direct staining of SCA-1 and CD31 staining). Slides were mounted with DAPI (ZSGB-BIO, Cat# ZLI-9557) when secondary antibodies had been cleaned with PBS (3 × 5 min).

Paraffin sections (5 μm) of articular repair samples were first dewaxed in xylene for 20 min, then rehydrated with 100%, 95%, 80%, 70%, and 50% alcohol gradients (each for 5 min) and immersed in PBS for 3 min. Later, these slides were treated with an antigen retrieval solution of pepsin (Sigma-Aldrich, Cat# R2283) and incubated at 37 ℃ for 30 min. Next, endogenous peroxidase was removed by 3% H_2O_2 for 15 min. When sections had been washed with PBS (3 × 5 min), slides were stained with anti-COL II antibody at 4 ℃ overnight. A secondary antibody (ZSGB-BIO, Cat# ZLI-9018) was added to the slides and incubated at room temperature for 1 h when the primary antibody had been removed by PBS (3 × 5 min). After cleaning the secondary antibody, DAB and hematoxylin staining were followed. At last, the sections were dehydrated with 80%, 95%, 100% alcohol, and xylene successively, then sealed with Mounting Medium. Alcian blue staining was also required on the rehydrated slides. Images were acquired with Leica TCS SP5II, Olympus VS200, and Wisleap WS-10 and analyzed by Image J software.

Single-cell preparation and scRNA sequencing of E10.5 MSX1$^+$ cells

About 20 hindlimb buds were dissected from E10.5 *Msx1*$^{P2A\text{-}tdTomato}$ mice. These limb buds were dissociated into single cells first and resuspended in PBS with 1% BSA. The sorted MSX1^{+} cells were both counted and adjusted to the concentration of about 1 × 10^{6}/mL. Then the suspension was centrifuged at 550 g for 5 min at 4 °C and repeated twice. Cells were counted and cell viability was confirmed by Countess II Automated Cell Counter (Thermo Fisher, Cat# AMQAX1000). Samples were then used for single-cell RNA sequencing (scRNA-seq) with the 10x Genomics system (Library preparation and sequencing were performed by Berry Genomics Inc, Beijing).

Processing of scRNA-seq raw sequencing data

The CellRanger software was obtained from the 10x Genomics website (https://www.10xgenomics.com/software). Alignment, filtering, barcode counting, and UMI counting were performed with the cell ranger count module to generate a feature-barcode matrix. scRNA-seq data of E10.5 MSX1^{+} mesenchymal progenitors has been submitted to the GEO database (GEO: GSE232586).

Reduction, clustering, and identification of differentially expressed genes in E10.5 mouse limb

The feature-barcode matrix was subsequently processed using R and

Seurat v4.2 package. We discarded cells that have unique features of fewer than 2200 and have counts of fewer than 6000. Subsequently, low-quality genes were identified as being expressed in less than 3 cells. The gene expression levels for each cell were normalized by the total expression, multiplied by a default size factor of 10,000, and log-transformed. Cell cycle effects were regressed with Seurat's function "ScaleData" using cell cycle markers. The dimensionality of the data was reduced by principal component analysis (PCA) (17 components) first and then data were clustered and visualized with UMAP (Uniform Manifold Approximation and Projection) on the 17 principal components (resolution = 0.7). Finally, the 7 cell clusters (LM, LPM, AER, SMCs, MCs, VECs, and Others） were then identified through cell-cluster-specific gene markers.

LPM and LM pseudotime analysis of mouse and human limb bud

Pseudotemporal ordering of LPM and LM cells was done with Monocle 3 v1.2.9. The data was further processed using UMAP with default parameters. A cluster graph was then created and partitioned to deduce disconnected trajectories. Subsequently, a principal graph in the low-dimensional space was generated and the pseudotime was calculated as the geodesic distance.

ScRNA-seq analysis of human 5 WPC limb

The processing of scRNA-seq raw sequencing data was consistent with mouse E10.5 data. The feature-barcode matrix was subsequently processed using R and Seurat v4.2 package.

We discarded cells that had unique features of fewer than 1,000 and had mitochondrial count percentages of more than 10%, low-quality genes were identified as being expressed in less than 3 cells. The gene expression levels for each cell were normalized by the total expression, multiplied by a default size factor of 10,000, and log-transformed. Cell cycle effects were regressed with Seurat's function "ScaleData" using cell cycle markers. Human 5 WPC limb scRNA-seq data of cs13 and cs15 (He et al., 2021) were integrated into a whole dataset according to Seurat's function "RunCCA". The dimensionality of the data was reduced by principal component analysis (PCA) (30 components) first and then data were clustered and visualized with UMAP on the 30 principal components (resolution = 0.4). Then we identified hindlimbs and separated LPM, and LM for downstream pseudotime analysis. AER cells were also characterized for Cellchat analysis.

Transcriptome analysis by RNA sequencing

RNA sequencing was conducted to investigate the gene expression profiles of the differentiated human day 8 $MSX1^{+}PDGFRA^{low}$ and $MSX1^{+}PDGFRA^{+}$ cells for FGF8+10 and Mock groups (n = 2), and 150

base pair paired-end reads were generated. The adaptors and low-quality reads from the raw reads of each sample were trimmed to obtain clean reads. The clean reads were mapped against the human genome (GRCh38) using HISAT2 v2.1.0. The expression level of each gene was quantified guided by reference annotation (GRCh38.104) using feature Counts v1.6.4. The PCA was analyzed and visualized by DESeq2 packages. RNA-seq data have been submitted to the GEO database (GEO: GSE232586).

Cell culture of hPSCs

Before the thawing, culture, and passaging of hPSCs, cell culture plates were coated with Matrigel (Corning, Cat# 354230) with a concentration of 1 mg/12mL in DMEM/F12 (Gibco, Cat# C11330500) at 37 ℃ for at least 1 h. Then the H1-hPSCs with clumps state were cultured and maintained in Pluripotency Growth Master 1 medium (PGM1, CELLAPY, Cat# CA1007500) in an incubator at 37 ℃ with 5% CO_2. When attaining subconfluency, the cells were dissociated into small clumps with TrypLE (Gibco, Cat# 12605028) and suspended in a PGM1 medium containing 10 μM Y27632 (MCE, Cat# HY10583). Y27632 was added to the PGM1 medium on the day of cell thawing and passage, and the fresh medium without Y27632 was replaced the next day. The medium was changed every day.

Generation of human *MSX1*$^{P2A\text{-}tdTomato}$ reporter cell line

The P2A-tdTomato-Loxp-PGK-Puro-Loxp cassette was inserted into the site before the stop codon of human *MSX1* by homology-directed repair (HDR) to achieve bicistronic expression of *MSX1* and tdTomato. The *MSX1* 5′ arm (642 bp) and 3' arm (503 bp) were amplified using PCR. P2A-tdTomato-Loxp-PGK-Puro-Loxp cassette, synthesized by BGI Genomics Co., Ltd, together with 5' arm and 3' arm were cloned to PUC19 plasmid to form the donor plasmid. The designed guide RNAs (gRNA, 5'-GCATGTACCACCTGACATAG-3') were combined with the *MSX1* stop codon and its 17 bp sequence of the 5' arm. These gRNA oligos were annealed into double-stranded and cloned into PX330 vector expressing Cas9 cassette, and then PX330-*MSX1*gRNA-Cas9 plasmid was constructed. 1 μg linearized donor plasmid with 1 μg PX330-*MSX1*gRNA-Cas9 plasmid were co-transfected into 1×10^5 H1-hPSCs by Lipofectamine stem reagent (ThermoFisher, Cat# STEM00015) using manufacturer's protocol. Puromycin screening was performed two days after transfection, and the screening lasted until no cell death was observed. When the confluency reached 80%, puromycin-resistant cells were cultured in 96-well plates to isolate the monoclonal cells and then expanded in 24-well plates or 12-well plates. To identify the genotypes of these monoclonal cell populations, the genome of screened cells was extracted using a Genomic Extraction kit (TIANGEN, Cat# DP304-03). The genome was

subsequently identified by PCR and sequencing. Three monoclonal cell lines were administered genotypic identification and one of them was stained by anti-OCT4 (Abcam, Cat# ab19857) and SOX2 (Abcam, Cat# ab97959) antibodies. It was proved that these cells maintained pluripotency during the process of cell line construction. Primers used in this section were listed in Table S2.

Differentiation of LPM and LM-like cells

The *MSX1*$^{P2A\text{-}tdTomato}$-hPSCs were digested by Accutase (STEM CELL, Cat# 07920) for 4 min into single cells. After counting, cells were suspended with PGM1 medium containing Y27632 and seeded in a new Matrigel-coated culture dish with a density of 1×10^4 cells per square centimeter. The medium containing Y27632 was removed and replaced with PGM1 medium the next day. The cells were washed with a wash medium (DMEM/F12 containing 3 mg/mL BSA and 1% Pen-Strep) to remove the residual PGM1 medium. Then cells were washed with CDMi basic medium (50% F12 (Gibco, Cat# 31765-035) + 50% IMDM (Gibco, Cat# 31980-030) + 1 mg/mL Poly(vinyl alcohol) (Sigma, Cat# P8136) + 450 μM Monothioglycerol (Sigma, Cat# M6145) + 0.7 μg/mL Insulin (Solarbio, Cat# I8830) + 15 μg/mL transferrin (Sigma, Cat# T0665) + 1% Pen-Strep + 1% Lipids concentrate (Gibco, Cat# 11905-031)). The MPS medium (CDMi medium + 50 ng/mL Activin A (Solarbio, Cat# P00101) +

6 μM CHIR99021 (MCE, Cat# HY-10182A) + 40 ng/mL BMP4 (R&D systems, Cat# 314-BP/CF) + 10 ng/mL FGF2 (Peprotech, Cat# 100-18B)) was added at day 0. On day 1, the MPS medium was replaced by LPM medium (CDMi medium + 60 ng/mL BMP4 + 1 μM CHIR99021). This process lasted for 3 days. The day 4 LPM was in an immature state and needed to continue differentiation in the LM medium (CDMi medium + 500 ng/mL FGF8 (MCE, Cat# HY-P70533) + 500 ng/mL FGF10 (MCE, Cat# HY-P4088). When the day 4 cells had been digested with TryPLE for 2 min, the wash medium was added to terminate the digestion. After centrifugation at 450 g for 3 min, the cells were resuspended in the LM medium and inoculated into Poly (2-hydroxyethyl methacrylate) (Sigma, Cat# P3932)-treated low-adhesion U-bottom 96-well plates with 2.5×10^5 cells per well.

To investigate the efficiency of different growth factors in promoting cell maturation to LM, CHIR99021 (6 μM) and FGF2 (500 ng/mL) were also added to the CDMi medium before inoculation, as CDMi medium was set as Mock control. Cells were centrifuged 300 g for 6 min and incubated at 37 ℃ for 24 h to promote pellet formation. On day 5 of collection, the pellets were placed on a low-adhesion 60 mm plate treated with Poly(2-hydroxyethyl methacrylate) and cultured for 3 days using the LM medium.

qRT-PCR

Total RNA was extracted from cells using Trizol reagent (ThermoFisher, Cat# 15596026) according to the manufacturer's instructions. cDNAs were prepared using the PrimeScript RT reagent kit (Takara Biomedical Technology, Cat# RR047A). The cDNAs were then used as templates for qPCR analysis with gene-specific primers. The qPCR was performed using a CFX384 real-time PCR system (BIO-RAD, USA). The cycle parameters were as follows: denaturation at 95 °C for 10 s, annealing at 60 °C for 30 s, and elongation at 72 °C for 30 s. The expression level of each gene was calculated using the 2ΔΔCt method. Primers used in qRT-PCR were listed in Table S3.

Osteogenic and chondrogenic differentiation assays

5 × 10^4 cells of the E10.5 subsets ($MSX1^+PDGFRA^{high}$, $Msx1^+PDGFRA^{medium}$, and $MSX1^+$ $PDGFRA^{low}$ cells) or the isolated MSCs cells were added into a 24-well plate to perform the osteogenic differentiation, the corresponding differentiation protocol has been described previously (Zhu et al., 2010). For the sorted human cells, 2.5 × 10^5 digested cells were cultured in a hole of 24-well plates. The osteogenesis process was performed in the osteogenic medium (α-MEM + 10% FBS + 100 nM dexamethasone (MCE, Cat# HY-14648) + 50 μg/mL L-ascorbate acid 2-phosphate (Sigma, Cat# A8960) + 10 mM β-glycerophosphate (Millipore, Cat# 35675-50GM) + 1% Pen-Strep) for

three weeks (medium was changed every 3 days) and identified by alizarin red staining.

The chondrogenic differentiation of 1×10^5 isolated primary $MSX1^+$ cells and MSCs was performed by micromass methods (ten Berge et al., 2008) and lasted for 3 weeks (the medium was changed every 3 days). The chondrogenic medium contained high glucose DMEM (Gibco, Cat# C11995500BT) supplemented with 10 ng/mL TGFβ3 (Peprotech, Cat# 100-36E), 30 ng/mL BMP4, 100nM dexamethasone, 50 μg/mL L-ascorbic acid-2-phosphate, 1 mM sodium pyruvate (Gibco, Cat# P5280), 40 μg/mL L-proline (Sigma-Aldrich, Cat# P0380) and 1 × ITS cell culture supplement (Thermofisher, Cat# 41400045). For the chondrogenesis of differentiated human cells, 1×10^5 cells were added into a sterile well of PCR 8-tube with culture medium (CDMi medium + 10 nM dexamethasone + 30 ng/mL BMP4 + 50 μg/mL L-ascorbate acid + 10 ng/mL TGFβ3 + 1 mM sodium pyruvate + 40 μg/mL proline + 1 × ITS). Four weeks later, these chondrogenic spheres were fixed in 4% PFA at 4 °C for 24 h and then dehydrated in 30% sucrose at 4 °C overnight. Alcian blue staining would be conducted to identify the chondrocytes.

Supplemental References

Fitzgerald, J., Rich, C., Burkhardt, D., Allen, J., Herzka, A.S., and Little,

C.B. (2008). Evidence for articular cartilage regeneration in MRL/MpJ mice. Osteoarthritis Cartilage 16, 1319-1326. 10.1016/j.joca.2008.03.014.

He, J., Yan, J., Wang, J., Zhao, L., Xin, Q., Zeng, Y., Sun, Y., Zhang, H., Bai, Z., Li, Z., et al. (2021). Dissecting human embryonic skeletal stem cell ontogeny by single-cell transcriptomic and functional analyses. Cell Res 31, 742-757. 10.1038/s41422-021-00467-z.

Nakao, K., Morita, R., Saji, Y., Ishida, K., Tomita, Y., Ogawa, M., Saitoh, M., Tomooka, Y., and Tsuji, T. (2007). The development of a bioengineered organ germ method. Nat Methods 4, 227-230. 10.1038/nmeth1012.

ten Berge, D., Brugmann, S.A., Helms, J.A., and Nusse, R. (2008). Wnt and FGF signals interact to coordinate growth with cell fate specification during limb development. Development 135, 3247-3257. 10.1242/dev.023176.

Zhu, H., Guo, Z.K., Jiang, X.X., Li, H., Wang, X.Y., Yao, H.Y., Zhang, Y., and Mao, N. (2010). A protocol for isolation and culture of mesenchymal stem cells from mouse compact bone. Nat Protoc 5, 550-560. 10.1038/nprot.2009.238